Molecular Therapy
Oncolytics
Original Article

Characterization of hypoxia response patterns identified prognosis and immunotherapy response in bladder cancer

Rui Cao,[1] Bo Ma,[2] Gang Wang,[3] Yaoyi Xiong,[4] Ye Tian,[1] and Lushun Yuan[5]

[1]Department of Urology, Beijing Friendship Hospital, Capital Medical University, Beijing 100050, China; [2]Department of Stomatology, Beijing Shijitan Hospital, Capital Medical University, Beijing 100038, China; [3]Department of Biological Repositories, Zhongnan Hospital of Wuhan University, Wuhan 430071, China; [4]Department of Urology, Zhongnan Hospital of Wuhan University, Wuhan 430071, China; [5]Department of Internal Medicine, Division of Nephrology, Leiden University Medical Center, 2333 ZA Leiden, the Netherlands

Intra-tumoral hypoxia and immunity are highly correlated with prognosis of tumor patients. Nonetheless, no studies have reported a systematic analysis of the relationship between hypoxia response and immunity in bladder cancer (BLCA). In this study, we comprehensively evaluated the hypoxia response patterns and their association with genomic and clinicopathological characteristics of 1,343 BLCA patients using unsupervised consensus clustering. Five hypoxia response patterns were defined, and the HPXscore was constructed using least absolute shrinkage and selection operator (LASSO)-Cox regression algorithms to represent the individual hypoxia response pattern. The low HPXscore group was characterized by immune activation and high DNA damage repair, which was referred to the immune-inflamed phenotype. However, activation of stromal-related pathways was observed in the high HPXscore group, which is recognized as T cell suppressive and more likely to be an immune-excluded phenotype. Furthermore, the HPXscore was an independent prognostic factor and could act as a good predictor for immunotherapeutic outcomes in BLCA. Thus, depicting a comprehensive landscape of the hypoxia characteristics may therefore help us to interpret the underlying mechanism of immune escape and shed light on the clinical application of hypoxia modification and immune checkpoints targeting immunotherapies for BLCA.

INTRODUCTION

Bladder cancer (BLCA) is the 10th most common cancer with an estimated 549,000 new cases and 200,000 deaths in 2018 around the world.[1] BLCA is divided into non-muscle-invasive BLCA (NMIBC) and muscle-invasive BLCA (MIBC) with different histology. Since Morales et al.[2] first reported that bacillus Calmette-Guérin (BCG) is effective in the treatment of NMIBC, it was approved as a first-line immunotherapeutic drug for NMIBC, indicating that BLCA was an immunogenic malignancy. However, not all NMIBC patients respond to BCG, and ~50% of non-responders will recur or progress to MIBC, with a 5-year survival rate of <50%. Moreover, MIBC is such a complex disease that the current staging and grading system could not guide the precision treatment efficiently, especially for immune checkpoints targeting immunotherapy treatment.[3]

However, many non-invasive biomarkers, such as UroVysion fluorescent *in situ* hybridization (FISH), Immunocyt, and nuclear matrix protein 22 (NMP-22), have been described and approved by the US Food and Drug Administration (FDA). However, low sensitivity and specificity hamper their ways to act as routine adjuncts or replacements for cystoscopy.[4] As a result, clinicians decided the treatment method mostly based on tumor stage, rather than on the biology and molecular characteristic of the disease. Recently, due to the development of biological or bioinformatics technology, our understanding of the underlying mechanism of the occurrence and development of BLCA has progressed. A comprehensive multi-platform genomic characterization by The Cancer Genome Atlas (TCGA) network and other independent cohorts have identified many distinct molecular subtypes, which are closer to the native biology of BLCA. Five classification systems have been widely accepted and described.[5–9] Although each group established their classification system based on special criteria and algorithms, each molecular subtype did have a unique characteristic or overlap between one another. All of this indicated that BLCA is a more extremely complex disease than what we previously recognized.

The tumor microenvironment (TME) is a complex system that contains numerous cell types and the factors they secrete. They cooperate with each other to generate a chronic inflammatory, immunosuppressive, and pro-tumoral environment, which is very important for tumor development and progression.[10,11] Hypoxia is characterized by lack of O_2 in an atmosphere where tissues are inadequately

Received 25 May 2021; accepted 22 June 2021;
https://doi.org/10.1016/j.omto.2021.06.011.

Correspondence: Ye Tian, Department of Urology, Beijing Friendship Hospital, Capital Medical University, Beijing 100050, China.
E-mail: urologisttianye@126.com
Correspondence: Lushun Yuan, Department of Internal Medicine, Division of Nephrology, Leiden University Medical Center, 2333 ZA Leiden, the Netherlands.
E-mail: l.yuan@lumc.nl

oxygenated.[12] In such a microenvironment, hypoxia acted as an essential metabolic element to shape cellular plasticity and tumor heterogeneity.[13] The rapid proliferation of tumor and dysregulated formation of the vasculature result in heterogeneously distributed areas of low oxygen pressure, inducing hypoxic stress. Under a hypoxic microenvironment, cells can adapt by regulating the hypoxia-inducible factor (HIF) family. HIFs are dimeric proteins consisting of an O_2-sensitive α subunit (HIF-1α, HIF-2α, or HIF-3α) and a scaffold β subunit (HIF-2β).[14] Under hypoxic stress, HIF dimers stabilize and translocate into the nucleus to induce the transcription and activation of numerous genes in regulating a variety of biological processes, including angiogenesis, proliferation, differentiation, and metabolism, among others. Many studies have reported that hypoxia is a trigger for cancer invasion and metastasis through activation of the hypoxia/HIF-1α cascade pathway.[15,16] Moreover, the adaptability to hypoxia allows for maintenance of cancer stem cells (CSCs) and survival of tumor. Moreover, chemotherapy-, radiotherapy-, or even immunotherapy-sensitive cancer cells might be transferred to resistant ones with long-term exposure to hypoxia.[17,18] Recent advances in immune checkpoint inhibitors (ICIs) have largely improved the prognosis of patients with advanced malignancy, such as non-small cell lung cancer (NSCLC), melanoma, and BLCA.[19–21] However, the high rate of non-responders also reminds us that the mechanism of immune escape is only partially understood. Hypoxia not only induces transcription factors or target genes to inhibit T cell proliferation and deactivate effector cytokine production directly,[22–24] but it also induces upregulation of co-inhibitory receptors, recruitment/conversion of immunosuppressive cell populations, and reconstruction of TME stroma to suppress immune system activation indirectly.[25–27]

In present study, we comprehensively evaluated the hypoxia characteristics and identified five hypoxia-response patterns (HPXclusters) with distinct survival advantage, TME immune cell infiltration, clinicopathological and genomic features by integrating 1,343 BLCA patients. As a result, we established a hypoxia phenotype-related gene signature (HPXscore), which is a set of scoring systems to quantify the hypoxia response pattern in individuals. The HPXscore was found to be a robust independent prognostic factor and predictive biomarker for the clinical response to ICIs in BLCA.

RESULTS

Characterization of hypoxia response patterns in BLCA

The construction scheme of hypoxia response patterns and hypoxia phenotype-related gene signature is shown in Figure 1A. We used the ConsensusClusterPlus package to select the optimal cluster numbers and found that there exist five distinct hypoxia response patterns in the meta-BLCA cohort (GEO: GSE13507, GSE32548, GSE62254, GSE32894, and GSE48075), as well as TCGA-BLCA cohort, including 165 cases in pattern A, 197 cases in pattern B, 235 cases in pattern C, 143 cases in pattern D, and 255 cases in pattern E, which were termed as HPXclusterA–HPXclusterE, respectively (Figure 1B). Unsupervised hierarchical clustering showed that the hypoxia response-related genes were differentially expressed among HPXclusterA–HPXclusterE in the meta-BLCA cohort (Figures 1C, S1A–S1C, and S2A–S2C). Furthermore, Kaplan-Meier survival curves demonstrated that prognoses of patients are significantly different among five HPXclusters (log-rank test, p = 0.0133; Figures 1D and S3) and that HPXclusterD exhibited a particularly prominent survival advantage compared with other patterns.

TME immune cell infiltration in distinct hypoxia response patterns

In order to find the association between TME and hypoxia response patterns, the relative amount of TME infiltration immune cells was calculated via a single-sample gene set enrichment analysis (ssGSEA) algorithm. Cluster heatmap analysis revealed that distinct HPXclusters exhibited distinct TME immune cell infiltration as follows (Figure 2A; Table S1): HPXclusterA was characterized by high TME immune cell infiltration with significant increases in the infiltration of activated B cells, B cells, mast cells, eosinophils, dendritic cells (DCs), and immature DCs; HPXclusterB was relatively less infiltrated but displayed a similar distribution to that of HPXclusterA; HPXclusterC featured low TME immune cell infiltration and only showed high infiltration of T central memory cells, T helper cells, and $CD56^{bright}$ natural killer cells; HPXclusterD was remarkably rich in effector TME immune cells infiltration, including activated CD4 cells, CD8 cells, DCs, and cytotoxic cells, but regulatory T (Treg) cells were also high infiltrated in this phenotype. Pearson correlation analysis indicated that Treg cells were significantly positively correlated with almost all immune cells, indicating the existence of a feedback loop regulation system within TME in BLCA (Figure S4). When effector TME immune cells were strikingly infiltrated, Treg cells would respond to them by increasing their amount to counter this phenomenon; HPXclusterE only infiltrated with activated CD4 T cells and type 2 T helper cells and exhibited remarkable decreases in other TME immune cell types.

Characteristics of the biological process in distinct hypoxia response patterns

We explored the biological process among five distinct patterns by performing ssGSEA for Kyoto Encyclopedia of Genes and Genomes (KEGG) pathways. As shown in Figures 2B, S5A–S5D, and Table S2, HPXclusterA was markedly activated in stromal and carcinogenic pathways such as the transforming growth factor (TGF)-β signaling pathway, WNT signaling pathway, and NOTCH signaling pathways; HPXclusterB displayed the similar trend with HPXclusterA, but it was less enriched in pathways in carcinogenic gene sets. HPXclusterC presented pathway enrichment associated with pathways in cancers, including the mTOR and TP53 signaling pathways, whereas HPXclusterD was annotated with pathways associated with immune activation, including the activation of antigen processing and presentation, the chemokine signaling pathway, cytokine-cytokine receptor interaction, natural killer cell-mediated cytotoxicity, and so on; HPXclusterE was prominently related to DNA damage repair-related pathways but was robustly negatively correlated with the immune activation biological process. However, we noticed that HPXclusterA was highly infiltrated with immune cells, but patients with this

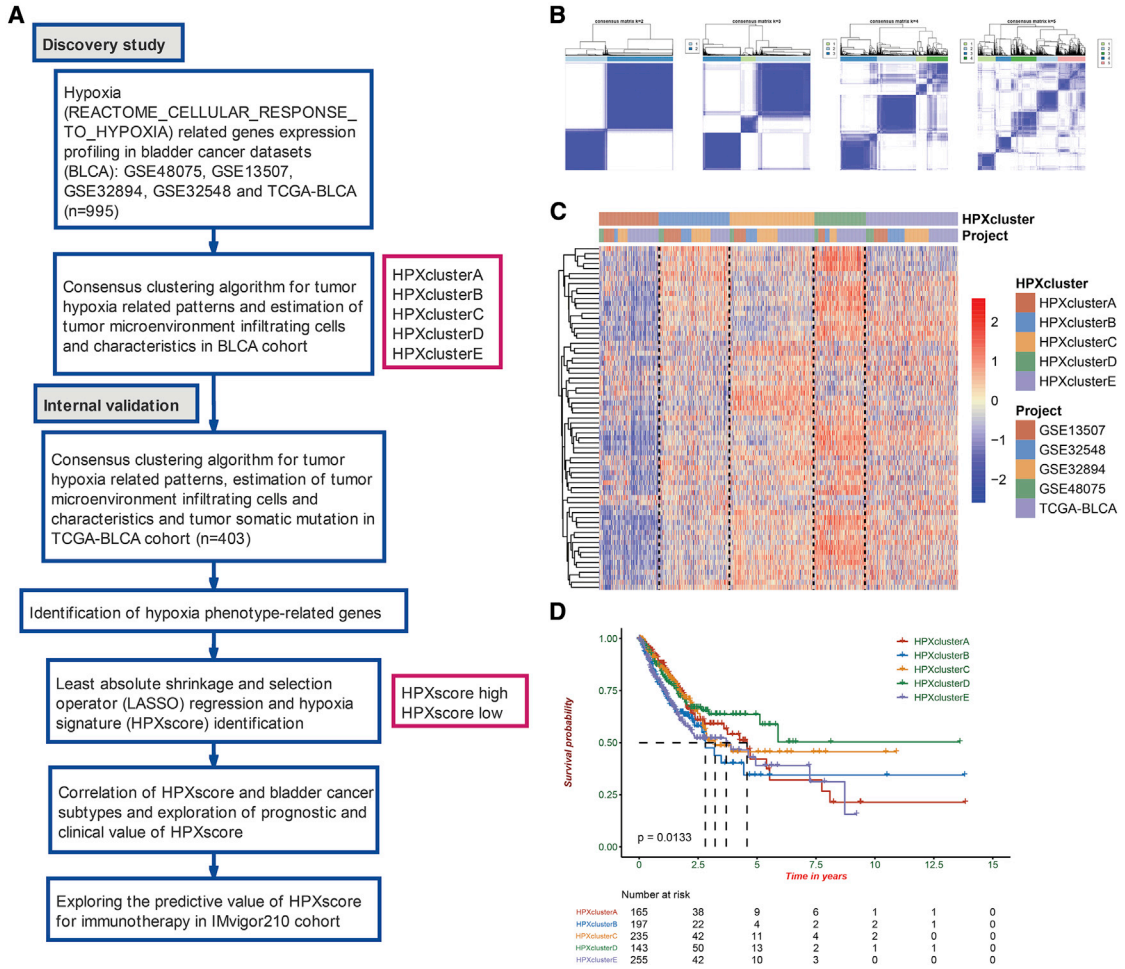

Figure 1. Consensus clustering of hypoxia response-related genes in bladder cancer

(A) Overview of study design. (B) Consensus matrices of patients in the meta-BLCA cohort (GEO: GSE13507, GSE32548, GSE32894, GSE48075, and TCGA-BLCA) for k = 2–5 using 1,000 iterations of unsupervised consensus clustering method (K-means) to ensure the clustering stability. (C) Hierarchical clustering of hypoxia response-related genes in meta-BLCA cohorts. Hierarchical clustering was performed with Euclidean distance and Ward linkage. The HPXclusters and BLCA cohorts are shown as patient annotations. Rows represented hypoxia response-related genes, and columns represented BLCA samples. Red represents high expression and blue represents low expression of each gene. (D) Survival analyses for the distinct hypoxia response patterns in the meta-BLCA cohort using Kaplan-Meier curves. The HPXclusterE showed significantly better OS than all other hypoxia response patterns (log-rank test, p = 0.0133).

phenotype did not show a matching survival advantage. Previous studies demonstrated that the TME immune cell infiltration pattern was divided into immune-desert, excluded, and inflamed phenotypes. The tumors with an immune-excluded phenotype were characterized by infiltration of abundant immune cells in the stroma surrounding the core tumor niche rather than penetrating their parenchyma, which was considered cytotoxic T cell suppressive.[28] Thus, we inferred that the stromal signaling pathway activation in patients with HPXclusterA might inhibit the anti-tumor effect of high effector immune cell infiltration. Then, ssGSEA of specific gene sets subsequently demonstrated that stromal-relevant signatures, including angiogenesis, epithelial-mesenchymal transition (EMT), and pan-fibroblast TGF-β response pathways, were significantly enhanced in HPXclusterA, which again confirmed our speculation (Figure 2C; Table S3). Moreover, we also found that HPXclusterD was remarkably enriched in CD8 T effector cells, antigen-processing machinery, and immune checkpoint signatures, but it was deactivated in the TGF-β/EMT signaling pathway (Figure 2C). Furthermore, we noticed a phenomenon that patients with HPXclusterD were highly infiltrated with activated DCs, DCs, and plasmacytoid DCs, but they showed a decrease in infiltration of immature DCs. DCs acted as a bridge connecting innate and adaptive immunity via antigen presentation and activation of naive T cells, which from another view answers the question of why HPXclusterD was highly activated in cellular immunity.[29] Then, we found that the expression levels of major histocompatibility complex (MHC) molecules, costimulatory molecules, and adhesion molecules, which were responsible for DC activation, were comprehensively elevated in HPXclusterD (Figure 2D). Then, we curated

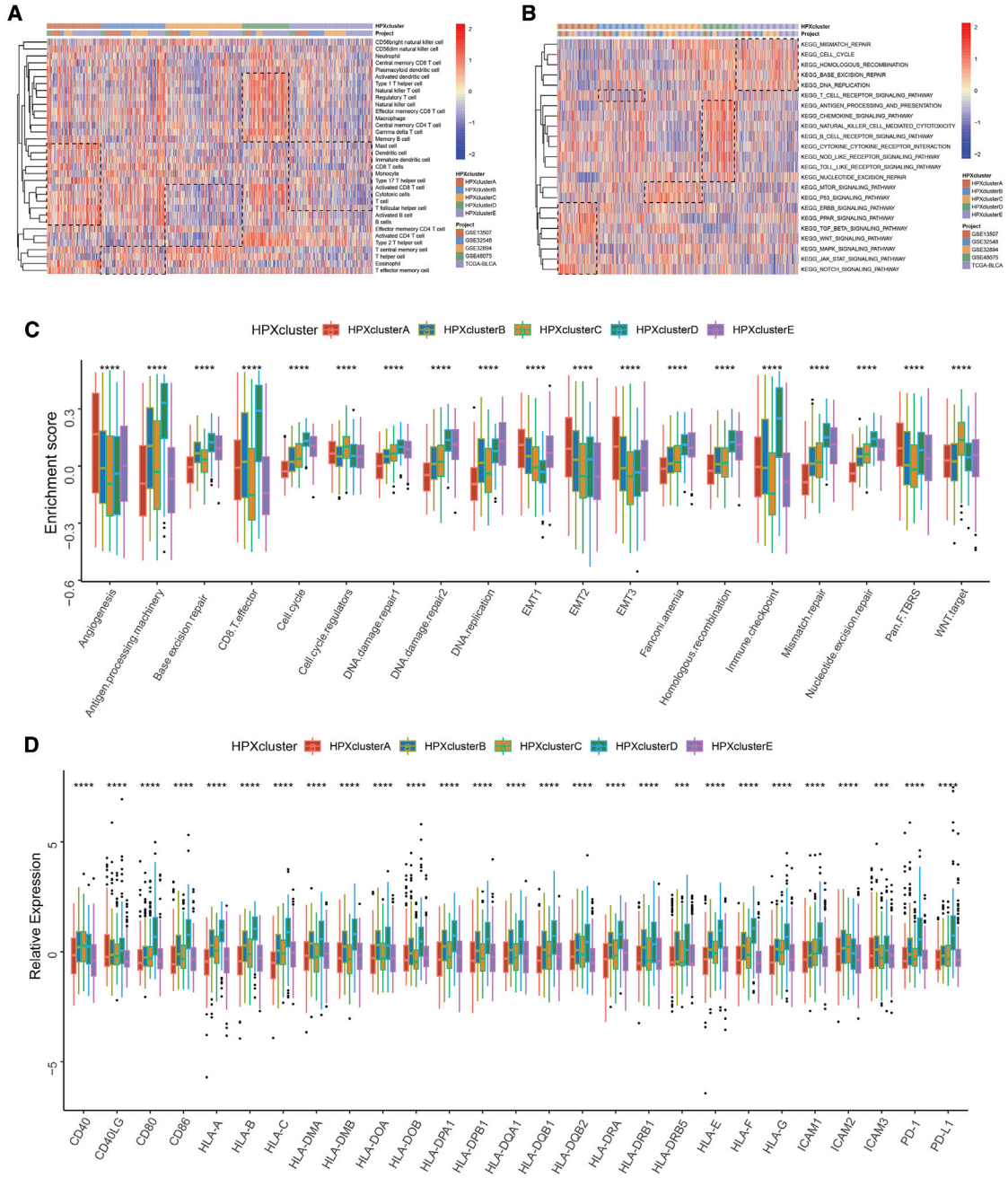

Figure 2. TME immune cell infiltration and biological process characteristics in distinct hypoxia response patterns

(A) Hierarchical clustering of TME infiltration immune cells for 995 patients in the meta-BLCA cohort. Rows represent relative amount of each immune cell, and columns represent BLCA samples. Red represents relative upregulated and blue represents relative downregulated of each immune cell. The HPXclusters and BLCA cohorts are shown as patient annotations. (B) ssGSEA showed the relative activity of biological pathways in distinct hypoxia response patterns in the meta-BLCA cohort. The heatmap was used to visualize indicated biological processes, including immune activation, antigen processing, mismatch repair, and pathway in cancers, etc. Red represents that the pathways were relatively activated and blue represents that the pathways were relatively suppressed in each sample. The HPXclusters and BLCA cohorts were used as sample annotations. (C) Difference in the enrichment of indicated signatures to represent specific biological processes including stromal-activation-relevant signatures, mismatch repair-relevant signatures, and immune activation-relevant signatures among five distinct hypoxia response patterns in the meta-BLCA cohort. (D) Differences in the expression levels of MHC molecules, costimulatory molecules, and adhesion molecules among five distinct hypoxia response patterns in the meta-BLCA cohort. In (C) and (D), the upper and lower ends of the boxes represent the interquartile range of values. The lines in the boxes represent the median value and the black dots show outliers. The statistical difference among five distinct hypoxia response patterns was tested by a one-way ANOVA test. ****$p < 0.0001$.

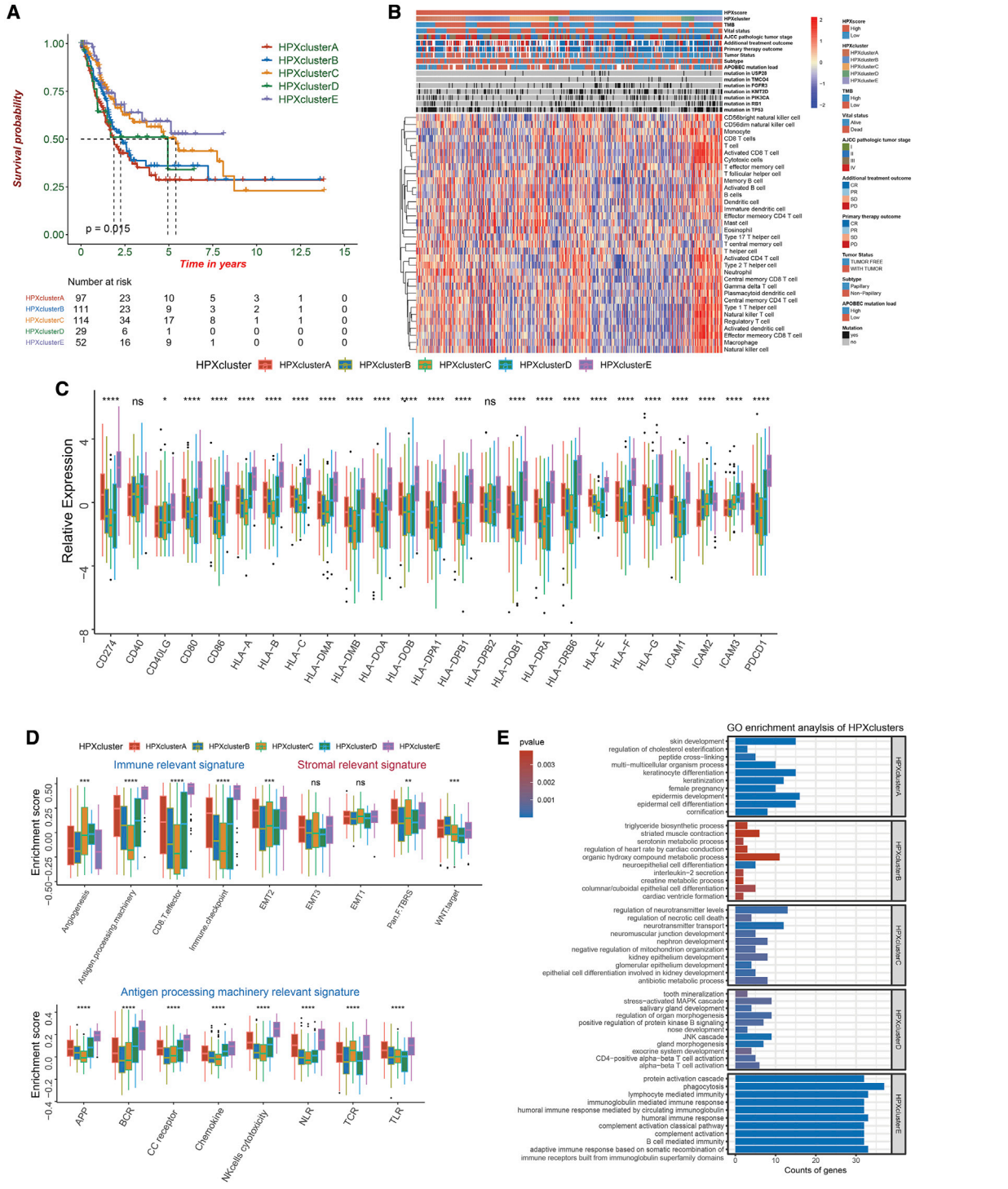

Figure 3. Characterization of hypoxia response patterns in TCGA-BLCA cohort

(A) Kaplan-Meier survival curves show the difference in prognosis advantage among five distinct hypoxia response patterns in TCGA-BLCA cohort (log-rank test, p = 0.015). (B) Hierarchical clustering of TME infiltration immune cells for 403 patients among five distinct hypoxia response patterns in TCGA-BLCA cohort. Rows represent relative amount of each immune cell, and columns represent BLCA samples. Red represents relatively upregulated and blue represents relatively downregulated of each immune cell. The HPXscore level, HPXclusters, TMB level, vital status, AJCC pathologic tumor stage, additional treatment outcome, primary therapy outcome, tumor status, histology subtype, APOBEC mutation load, and mutation in indicated genes were used as sample annotations. (C) Difference in the expression of MHC molecules, costimulatory

(legend continued on next page)

the markers representative of the major signaling pathways in immune phenotypes as follows: immune activation: CD8A, CXCL10, CXCL9, GZMA, GZMB, IFNG, PRF1, TBX2, and TNF; immune checkpoints: CD80, CD86, cytotoxic T lymphocyte-associated protein 4 (CTLA-4), IDO1, LAG3, programmed death-1 (PD-1), programmed death-ligand 1 (PD-L1), PD-L2, TIGIT, and TIM-3; and TGF-β/EMT signaling pathway: ACTA2, COL4A1, PDGFRA, SMAD9, TGFB2, TGFBR2, TWIST1, VIM, and ZEB1. The results demonstrated a similar trend to the biological process and pathway enrichment among different patterns measured by ssGSEA (Figure S6A–S6C). Thus, we found that five hypoxia response patterns had a very differential characteristic of TME immune cells infiltration phenotype that HPXclusterA/B was featured by highly immune cell infiltration and stromal activation and more likely to be an immune-excluded phenotype; HPXclusterD was characterized by full immune activation with infiltration with effector immune cells and would be recognized as an immune-inflamed phenotype, whereas HPXclusterC/E was suspected as an immune-desert phenotype, characterized by the suppression of immunity.

Hypoxia response patterns in the TCGA-BLCA cohort

To further explore the correlation between hypoxia response phenotypes and clinical traits as well as biological behaviors, we then mainly focused on TCGA-BLCA cohort, which comprised comprehensive clinicopathological and molecular parameters. Similar to the meta-BLCA cohort, unsupervised consensus clustering also identified five distinct HPXclusters in TCGA-BLCA cohort (Figure S7A). The hypoxia response transcriptional profile was differentially distributed among five HPXclusters (Figure S7B). Notably, five HPXclusters showed significantly differences in survival advantage, indicating that HPXclusterC/E was associated with better prognosis while HPXclusterA/B was associated with poorer prognosis (log-rank test, $p = 0.015$; Figures 3A and S8).

Then, we wanted to figure out whether the survival advantage of HPXclusterC/E was relevant to clinicopathological characteristics, such as tumor-lymph node-metastasis (TNM) stage and therapy outcome. Unfortunately, the results demonstrated that there was no significant difference in TNM stage and primary therapy outcome among the five HPXclusters. However, we then found that the patients with HPXclusterC/E were more likely to be tumor free and have an additional treatment outcome of complete response (CR)/partial response (PR) and living status (Figure S9). As the survival benefits were not correlated with the TNM stage, we inferred that they might be caused by differences in TME immune cell infiltration. Therefore, we were surprised to find that HPXclusterE of TCGA-BLCA cohort exhibited a similar TME immune cell distribution to that of HPXclusterD in the meta-BLCA cohort, which was characterized by high effector TME immune cell infiltration, including activated CD4 cells, CD8 cells, DCs, cytotoxic cells, and so on, but HPXclusterC of TCGA-BLCA cohort was significantly less infiltrated compared with HPXclusterE (Figure 3B; Table S4). Furthermore, HPXclusterE also remarkably accumulated with activated DCs, DCs, and plasmacytoid DCs, but showed a lack of immature DCs, accompanied by upregulation of MHC molecules, costimulatory molecules, and adhesion molecules (Figure 3C). Moreover, the pathway annotation revealed that the immune activation and antigen-processing machinery-relevant signatures were significantly enhanced in HPXclusterE but not in HPXclusterC. HPXclusterA was found to be enriched in a stromal signaling-relevant signature (Figure 3D; Table S5). Then, subsequent ssGSEA of KEGG demonstrated that HPXclusterE was deactivated in TGF-β, WNT, p53, mTOR, and PPAR signaling pathways but enriched in DNA damage repair signaling pathways (Figures S10A–S10C; Table S6). The expression levels of immune activation, immune checkpoints, and TGF-β/EMT signaling pathway markers were distributed in the same way as displayed in the function annotation among the five distinct HPXclusters (Figures S11A–S11C). In order to further explore the potential biological process of each HPXcluster, differentially expressed genes (DEGs) were determined by comparing each cluster with others (Figure S12A; Table S7). Then, the DEGs of each cluster were used to perform Gene Ontology (GO) enrichment analysis through the clusterProfiler package, and the significant changes in GO terms were summarized (Table S8). Surprisingly, HPXclusterA was enriched in keratinocyte differentiation and keratinization, which was considered to be stromal signaling pathway activation; HPXclusterC was significantly enriched in pathways associated with epithelium development, which might be the cause of good prognosis; and HPXclusterE was strikingly enriched in the pathway related to immune activation (Figure 3E). All of these findings again suggested that hypoxia plays an indispensable role in immune regulation within the TME.

Tumor somatic mutation in distinct hypoxia response patterns

We next investigated the distribution differences of somatic alterations among different HPXclusters in BLCA using the packages maftools and complexheatmap. By analyzing the Mutect2 mutation annotation files of TCGA-BLCA cohort, waterfall plots integrated with 30 highly variant mutant genes were utilized to show the mutation landscape. As shown in Figure 4A, the mutation rate of the top 30 mutated genes was highest in HPXclusterE, especially for TP53 and RB1, which was considered to be responsible for the sensitivity of ICIs in tumor patients (Figure 4A).[30,31] Moreover, we found that HPXclusterE was markedly correlated with a higher tumor mutation burden (TMB), while HPXclusterB was associated with the lowest

molecules, and adhesion molecules among five distinct hypoxia response patterns in TCGA-BLCA cohort. (D) Difference in the enrichment of immune-relevant signatures, stromal-relevant signatures, and antigen processing machinery-relevant signatures among five distinct hypoxia response patterns in TCGA-BLCA cohort. In (C) and (D), the upper and lower ends of the boxes represent interquartile range of values. The lines in the boxes represent median value, and the black dots show outliers. The statistical difference among five distinct hypoxia response patterns was tested by a one-way ANOVA test. *$p < 0.05$, **$p < 0.01$, ***$p < 0.001$, ****$p < 0.0001$. (E) Gene Ontology (GO) enrichment analysis of the DEGs among distinct hypoxia patterns. The length and color depth of the bar represent the number of genes enriched and the p value of each GO term, respectively.

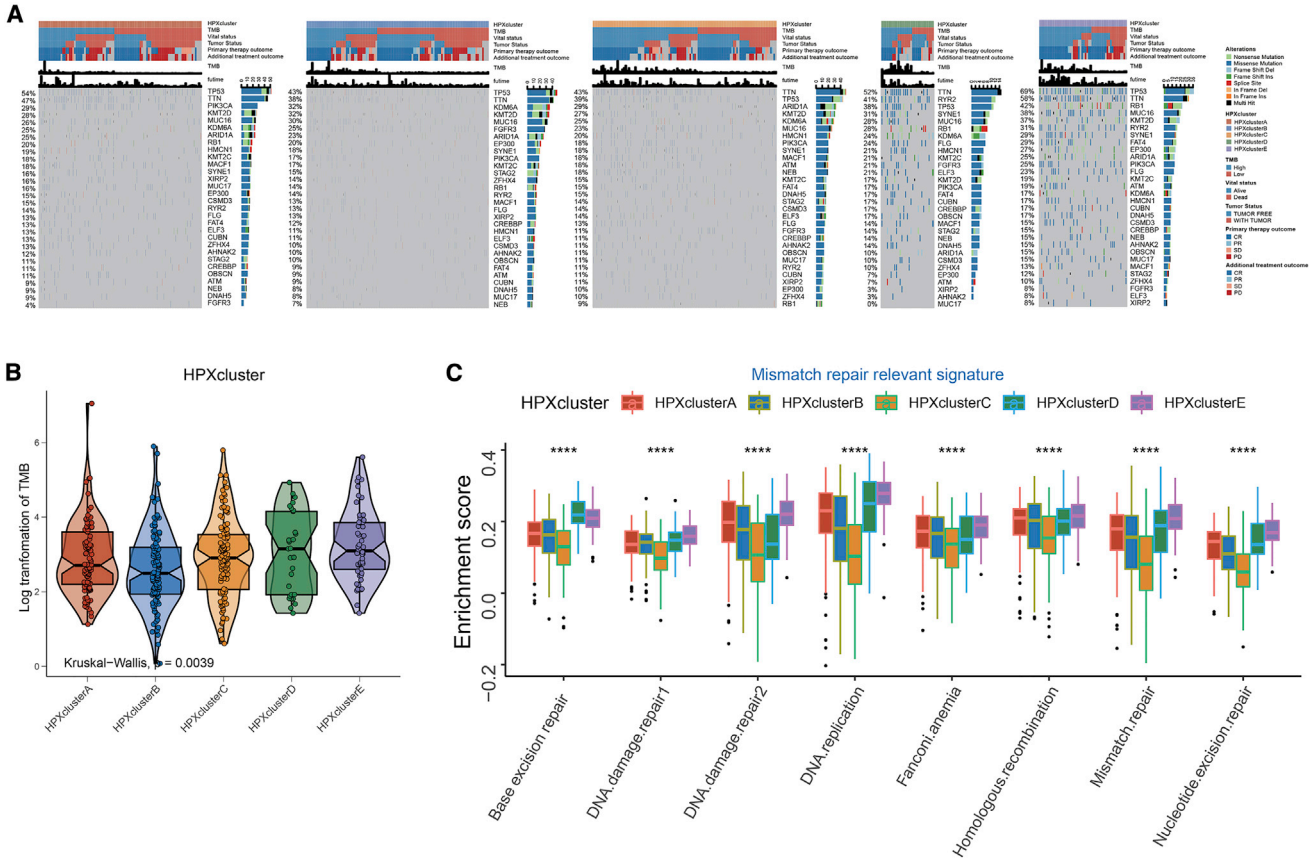

Figure 4. Tumor somatic mutation landscape of distinct hypoxia response patterns in TCGA-BLCA cohort

(A) Distribution of the top 30 variant mutated genes among five distinct hypoxia response patterns for BLCA. The genetic alterations types were indicated in the waterfall plot annotation. The upper barplots indicated TMB and overall survival (OS) time. The numbers on the left and right bar plots show the mutation frequency of each gene in distinct hypoxia response patterns. The HPXcluster, TMB, vital status, tumor status, primary therapy outcome, and additional treatment outcome are shown as patient annotations. (B) Differences in TMB among different hypoxia response patterns. The upper and lower ends of the boxes represent the interquartile range of values. The lines in the boxes represent the median value. A Kruskal-Wallis test was used to compare the statistical difference between each pattern ($p = 0.0039$). (C) Differences in the enrichment of mismatch repair-relevant signatures among five distinct hypoxia response patterns in TCGA-BLCA cohort. The upper and lower ends of the boxes represent the interquartile range of values. The lines in the boxes represent the median value, and the black dots show outliers. The statistical difference among five distinct hypoxia response patterns was tested by a one-way ANOVA test. ****$p < 0.0001$.

TMB (Figure 4B). Furthermore, the functional annotation of specific gene sets revealed that the enrichment of mismatch repair signaling pathway signatures, such as base excision repair, DNA damage repair, mismatch repair, and nucleotide excision repair, were remarkably enhanced in HPXclusterE (Figures 4C and S10A; Table S9). All of these findings indicated that hypoxia response patterns not only distinguished the TME immune cell infiltration, but they were also correlated with the mutation landscape, which again underlies the importance of hypoxia in BLCA development.

Construction of the hypoxia phenotype-related gene signature

Although hypoxia played a key role in shaping different TME landscapes, it was not convenient to predict the hypoxia response pattern in individual, as all of the above analyses were conducted on the population. Considering the individual heterogeneity and complexity of hypoxia response patterns, we aimed to construct a set of a scoring system to quantify the hypoxia response pattern of the individual in BLCA, which was termed the HPXscore. To depict the hypoxia response patterns through transcriptomic data, 2,257 phenotype-related meta-DEGs were determined by merging DEGs in each HPXcluster (Figure S12; Table S7). Based on univariate Cox regression analyses, 394 of 2,257 meta-DEGs related with prognosis were finally defined as hypoxia phenotype-related prognostic candidate genes (Table S10). Then, least absolute shrinkage and selection operator (LASSO)-Cox regression analyses were performed on those genes for dimension reduction to develop a hypoxia phenotype-related gene signature (HPXscore) that could better represent the hypoxia response pattern. Finally, 12 genes were enrolled to establish the HPXscore, and their coefficients are shown in Table S11.

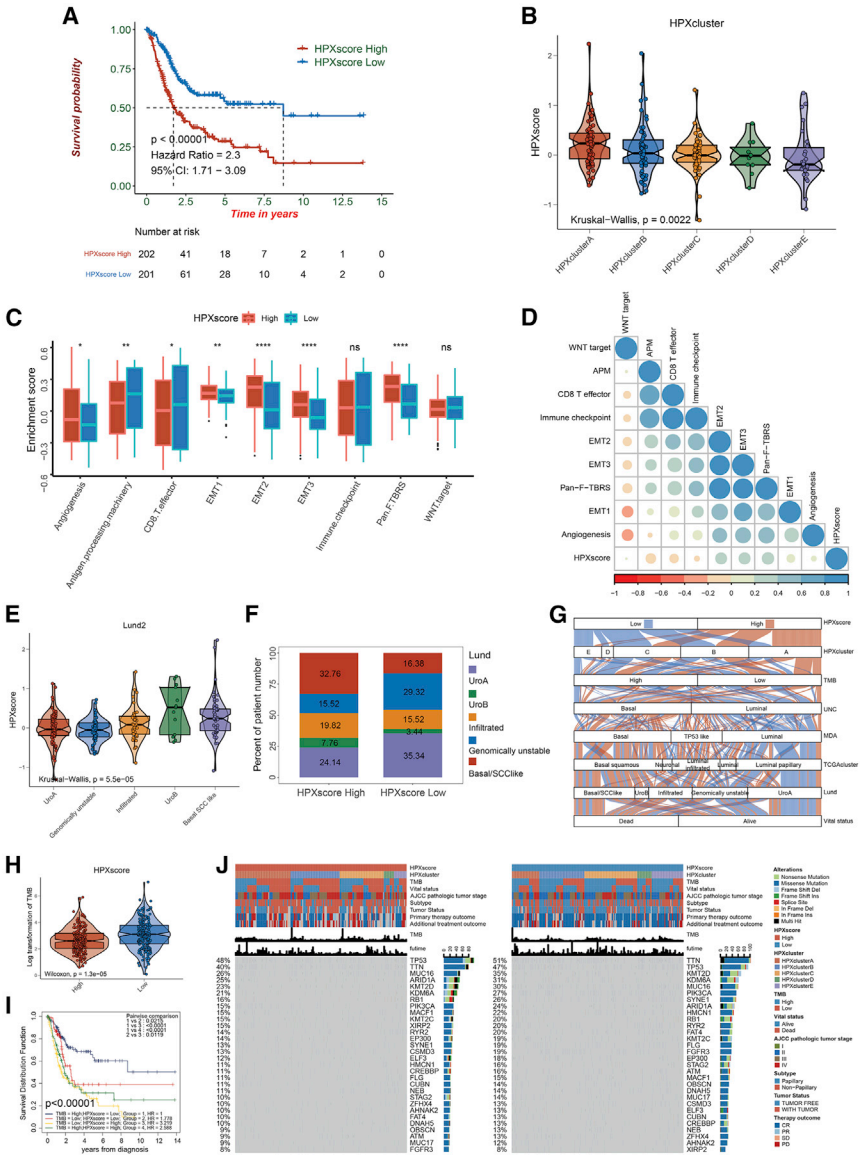

Figure 5. Transcriptome traits and biological characteristics of hypoxia phenotype-related gene signature (HPXscore) in TCGA-BLCA cohort

(A) Kaplan-Meier survival curves showed the difference in prognosis advantage between high and low HPXscore groups in TCGA-BLCA cohort (log-rank test, $p < 0.00001$). (B) Distributions of HPXscore in five distinct hypoxia response patterns. Kruskal-Wallis test was used to compare the statistical difference between each pattern ($p = 0.0022$). (C) Differences in the enrichment of immune activation-relevant signatures and stromal activation-relevant signatures between high and low HPXscore groups in TCGA-BLCA cohort. The upper and lower ends of the boxes represent the interquartile range of values. The lines in the boxes represent the median value, and the black dots show outliers. The statistical difference between high and low HPXscore groups was tested by a Student's t test. *$p < 0.05$, **$p < 0.01$, ****$p < 0.0001$. (D) Correlation between HPXscore and gene signatures linked to immune and stromal activation in TCGA-BLCA cohort. Negative correlation is marked with blue and positive correlation is marked with red. (E) Differences in HPXscore between different molecular subtypes in the Lund classification system. The Kruskal-Wallis test was used to compare the statistical difference between different molecular subtypes ($p = 5.5e{-}5$). (F) Proportion of Lund molecular subtypes in high and low HPXscore groups in TCGA-BLCA cohort. The statistical difference was measured with a Fisher's exact test ($p = 0.004467$). (G) Alluvial diagram showing the changes of HPXscore, HPXclusters, TMB, indicated molecular subtypes, and vital status in TCGA-BLCA cohort. (H) Differences in TMB between high and low HPXscore groups in TCGA-BLCA cohort. The TMB was $\log_2$ transformed. The statistical difference was measured with the Wilcoxon test ($p = 1.3e{-}5$). (I) Kaplan-Meier survival curves show the difference in prognosis advantage among four groups stratified by HPXscore and TMB in TCGA-BLCA cohort (log-rank test, $p < 0.00001$). (J) Distribution of top 30 variant mutated genes between high and low HPXscore groups in TCGA-BLCA cohort. The genetic alteration types are indicated in the waterfall plot annotation. The upper bar plots indicate TMB and OS time. The numbers on the left and right bar plots show the mutation frequency of each gene in distinct hypoxia response patterns. HPXscore, HPXcluster, TMB, vital status, AJCC pathologic tumor stage, subtype, tumor status, primary therapy outcome, and additional treatment outcome are shown as patient annotations.

Next, we assigned the patients into low or high HPXscore groups at the median cut-off to identify the value of the HPXscore in predicting patients' outcomes. Kaplan-Meier survival curves indicated that patients with a low HPXscore demonstrated a prominent survival benefit (log-rank test, $p < 0.00001$; Figure 5A), with the 5-year survival rate twice than that for patients with a high HPXscore (53.2% versus 27.1%). This was also validated in the meta-BLCA cohort (log-rank test, $p = 0.0032$; Figure S12B). A Kruskal-Wallis test revealed a significant difference on HPXscore among HPXclusters that harmful HPXclusterA showed the highest median score while beneficial HPXclusterE displayed the lowest median score (Kruskal-Wallis test, $p = 0.0022$; Figure 5B). Function annotation was performed to better illustrate the characteristics of the hypoxia phenotype-related gene signature. The results showed that patients with a low HPXscore were enriched in the immune activation signature such as CD8 T effectors and antigen-processing machinery, while patients in the high HPXscore group were significantly associated with enhanced enrichment of stromal pathways, including angiogenesis, EMT, and pan-fibroblast TGF-β response pathways (Figure 5C). The Pearson correlation analyses between the curated signatures and the

HPXscore also validated our findings (Figure 5D). The above results strongly suggested that a low HPXscore was significantly associated with immune activation, whereas a high HPXscore was highly correlated with stromal activation. We next aimed to determine the correlation between HPXscore and clinical traits and molecular subtypes. We found that patients with a high HPXscore were more likely to be patients with non-papillary, more advanced American Joint Committee on Cancer (AJCC) pathologic TNM stage, lympho-vascular invasion, and lymph node-positive detection, as well as treatment outcome of stable disease (SD)/progressive disease (PD) and dead status. However, the opposite patterns were observed in the low HPXscore group (Figure 3B; Table S12). A comprehensive molecular landscape has been constructed for BLCA by TCGA and other independent groups, which classified BLCA into many different molecular subtypes. Furthermore, we evaluated the difference of HPXscore among these molecular subtypes. Surprisingly, we found that patients with a low HPXscore accumulated in molecular subtypes of luminal, luminal papillary, TCGA I/II, urothelial-like A (UroA), and genomically unstable (GU), which were related with low malignancy and better survival. However, molecular subtypes with basal, basal squamous, TP53-like, TCGA III/IV, and basal/SCC-like, which were characterized by high malignancy and worse prognosis, were significantly concentrated in the high HPXscore group (Figures 5E, 5F, and S13A–S13F). Then, the distribution changes of molecular subtypes in individual were visualized with an alluvial diagram (Figure 5G).

We noticed that patients with GU subtype showed the lowest HPXscore compared to other molecular subtypes within the Lund classification system (Kruskal-Wallis test, $p = 5.5e{-}5$, Figure 5E). Additionally, the numbers of patients with the GU subtype were about double in the low HPXscore group compared with those with a high HPXscore (Fisher's exact test, $p = 0.004467$, Figure 5F). In the above results, we found that five hypoxia response patterns were remarkably different in mutated gene distribution and TMB quantification. Because the GU subtype was characterized by high mutation frequency, we next analyzed the distribution differences of somatic mutation between low and high HPXscores in TCGA-BLCA cohort. We found that PI3KCA, KMT2D, and FGFR3 were highly mutated in patients with a low HPXscore, but there was no significant difference of mutation in TP53 and RB1 between the high and low HPXscore groups (Figure 5J). APOBEC mutagenesis is reported to be associated with increased expression of immune signatures, including the interferon signaling pathway.[32] Thus, the APOBEC mutation load was strikingly increased in the low HPXscore group when compared with the high HPXscore group (Figure 3B; Table S12). Moreover, we found that patients with a low HPXscore were markedly correlated with a higher TMB compared with patients in the high HPXscore group, indicating that the HPXscore and TMB exhibited a significant negative correlation (Wilcoxon test, $p = 1.3e{-}5$, Figure 5H). Clinical trials as well as preclinical studies reported that higher TMB was associated with long-term survival and durable clinical benefit, especially when treated with ICIs. Next, we stratified all of the patients into four groups based on the levels of HPXscore and TMB. Furthermore, Kaplan-Meier survival curves indicated that patients with a low HPXscore displayed a significant survival advantage regardless of whether the TMB was high or low (log-rank test, $p < 0.00001$, Figure 5I).

The HPXscore can be utilized as an independent prognostic factor in BLCA

As the HPXscore was significantly correlated with high malignancy and played a vital role in BLCA tumorigenesis, we sought to determine whether the HPXscore was a clinically independent prognostic factor for BLCA patients through univariate and multivariate Cox regression analyses. The HPXscore and TMB, together with other clinical features, including age, sex, histological subtype, AJCC pathological T stage, pathological N stage, pathological M stage, and pathological tumor stage, were enrolled as covariates to perform the analysis. The results demonstrated that the HPXscore, TMB, pathological T stage, pathological N stage, and age were independent factors that could be utilized to predict the prognosis of BLCA patients (Figures 6A and 6B). By combining the independent prognostic factors, we constructed a nomogram that serves as a clinically relevant quantitative method by which clinicians can predict mortality in BLCA patients (Figure 6C). Every patient would be assigned a total point value by adding the points for each prognostic parameter. Higher total points correspond to a worse patient outcome. Furthermore, calibration plots indicated that the nomogram had a similar performance to that of an ideal model (Figures 6D and 6E). Decision curve analysis (DCA) also revealed that the nomogram had high potential clinical utility (Figures 6F and 6G).

HPXscore was a predictive biomarker for clinical response to ICI immunotherapy

Accumulated evidence demonstrates that immunotherapies based on ICIs have undoubtedly emerged as a major breakthrough in cancer treatment. As a negative correlated with TMB and was significantly associated with immune and stromal activation, the role of the HPXscore in mediating the clinical response to ICI treatment was indirectly confirmed. We next explored whether the HPXscore could predict immunotherapeutic benefits in BLCA by using an IMvigor210 (mUC) cohort, which consisted of patients with metastatic urothelial cancer (mUC) receiving PD-L1 inhibitor with atezolizumab. Kaplan-Meier survival curves revealed that patients with a low HPXscore exhibited significant clinical benefits and markedly prolonged survival when compared with the high HPXscore group (log-rank test, $p < 0.001$, Figure 7A). Surprisingly, function annotation showed that immune activation signatures such as CD8 T effectors, antigen-processing machinery, and immune checkpoints were remarkably enriched in the low HPXscore group, while stromal signatures including EMT/TGF-β and WNT/target pathways were highly activated in patients with a high HPXscore (Figure 7B). Then, the correlation matrix showed that the HPXscore exhibited a positive correlation with a stromal-relevant signature and negative correlation with an immune activation-relevant and mismatch repair signature (Figure 7C).

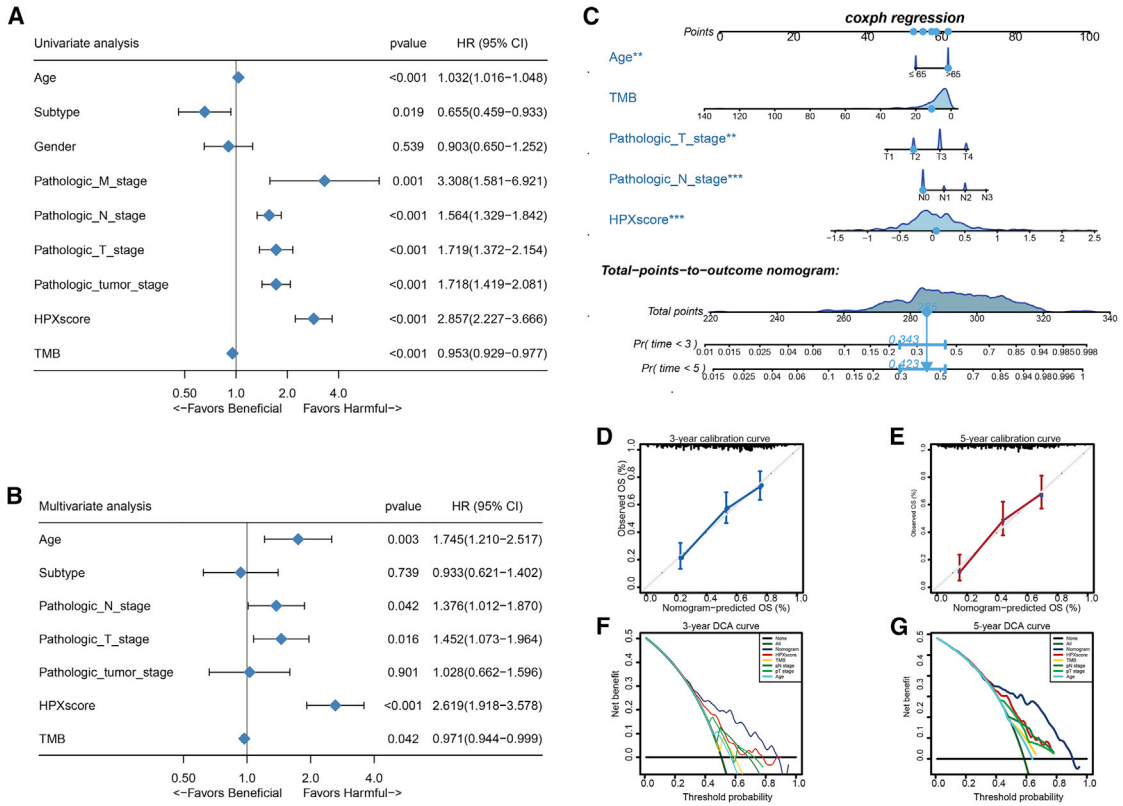

Figure 6. HPXscore is an independent prognosis factor in the nomogram

(A and B) Forest plot summary of the univariate (A) and multivariable (B) Cox analyses of the HPXscore and clinicopathological characteristics. The results indicate five independent prognosis factors, including age, pathologic T stage, pathologic N stage, TMB, and HPXscore. The blue diamond squares on the transverse lines represent the HR, and the black transverse lines represent the 95% confidence interval (CI). The p value and 95% CI for each clinical feature are displayed in detail. (C) Nomograms for predicting the probability of patient mortality at 3 or 5 year OS based on five independent prognosis factors. **p < 0.01, ***p < 0.001. (D and E) Calibration curves of the nomogram for predicting the probability of OS at 3 and 5 years. (F and G) Decision curve analyses (DCAs) of the nomograms based on five independent prognosis factors for 3-year and 5-year risk.

Moreover, a previous study utilizing the IMvigor210 (mUC) cohort demonstrated that patients within the GU subtype in the Lund classification system, as well as the II subtype in TCGA classification system, were more likely to respond to treatment with ICIs. Our data indicated that that GU subtype and II subtype showed the lowest HPXscore compared to other molecular subtypes in each classification system, which is consistent in our previous findings in TCGA-BLCA cohort (Kruskal-Wallis test, p = 1.6e−9, Figure 7D, and Kruskal-Wallis test, p = 1.5e−11, Figure S14B). Moreover, the numbers of the GU subtype in patients with a low HPXscore group were more than 3-fold those in the high HPXscore group (Fisher's exact test, p = 0.005722, Figure 7E). Additionally, the numbers of the II subtype were more than twice those in the low HPXscore group when compared with the high HPXscore group (Fisher's exact test, p = 0.000404, Figure S14A). Then, the alluvial diagram was utilized to show distribution changes of molecular subtypes, vital status, and overall response in individual in the IMvigor210 (mUC) cohort (Figure 7F).

Furthermore, we also found a strikingly negative correlation of TMB and HPXscore in the IMvigor210 (mUC) cohort (Wilcoxon test, p = 0.0028, Figure 8A, and Fisher's exact test, p = 0.001859, Figure 8B). Kaplan-Meier survival curves suggested that a low HPXscore/high TMB group showed a great survival advantage compared with the other groups (log-rank test, p < 0.00001, Figure 8C). Next, we found that immune activation, immune checkpoint, and MHC molecular relevant genes were highly upregulated, while the TGF-β-EMT pathway-relevant genes were significantly downregulated in the low HPXscore group (Figures 8D, 8E, S14D, and S14E). The opposite patterns were seen in the high HPXscore group. Then, the difference of the immune checkpoint PD-L1 located on tumor cells or immune cells between the low or high HPXscore groups was measured, as it was also associated with the clinical response of immunotherapy. Our data showed that patients with IC2 exhibited the lowest HPXscore, and there were more patients with the IC2 phenotype in the low HPXscore group (Figures S14G and S14H). However, we did not find any difference in TC distribution between high and low HPXscore levels (Figure S14F).

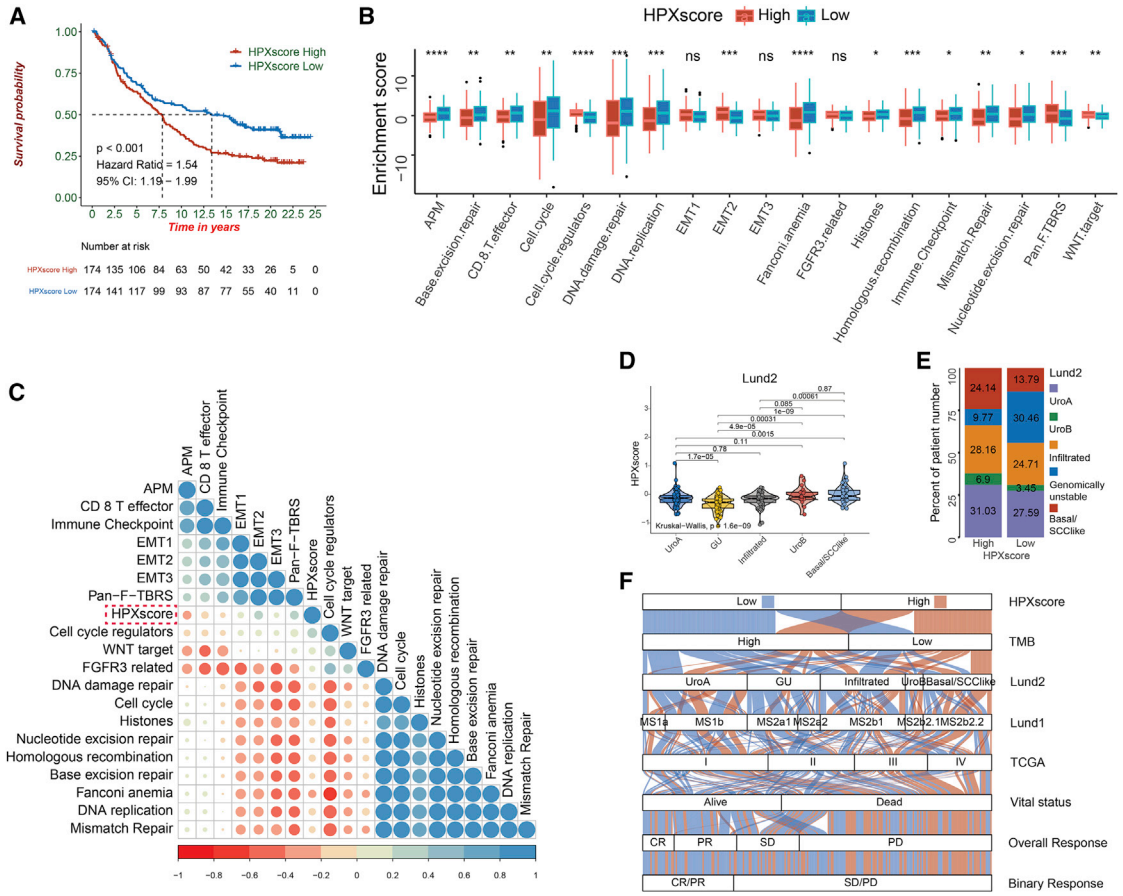

Figure 7. Characteristics of HPXscore in IMvigor210 (mUC) cohort

(A) Kaplan-Meier survival curves show the difference in prognosis advantage between high and low HPXscore groups in the IMvigor210 (mUC) cohort (log-rank test, $p < 0.001$). (B) Difference in the enrichment of the indicated gene signature (curated from IMvigor210 [mUC] cohort) between high and low HPXscore groups in the IMvigor210 (mUC) cohort. The upper and lower ends of the boxes represent the interquartile range of values. The lines in the boxes represent median value, and the black dots show outliers. The statistical difference between high and low HPXscore groups was tested by the Student's t test. *$p < 0.05$, **$p < 0.01$, ***$p < 0.001$, ****$p < 0.0001$. (C) Correlation between HPXscore and indicated gene signature in IMvigor210 (mUC) cohort. Blue indicates negative correlation and red indicates positive correlation. (D) Differences in HPXscore among different molecular subtypes in the Lund classification system in IMvigor210 (mUC) cohort. The Kruskal-Wallis test was used to compare the statistical difference between different molecular subtypes ($p = 1.6e{-}9$). (E) The proportion of Lund molecular subtypes in high and low HPXscore groups in the IMvigor210 (mUC) cohort. The statistical difference was measured with the Fisher's exact test ($p = 0.005722$). (F) Alluvial diagram showing the changes of HPXscore, TMB, indicated molecular subtypes, vital status, ICI overall response, and binary response in the IMvigor210 (mUC) cohort.

We previously found that hypoxia response patterns and HPXscore played a non-negligible role in shaping the immune TME landscape based on distinct immune phenotypes. In this study, we validated the role of the HPXscore in determining different immune phenotypes in the IMvigor210 (mUC) cohort, which contained complete information on immune phenotypes. Interestingly, we found that the patients with an inflamed phenotype remarkably accumulated in the low HPXscore group (Fisher's exact test, $p = 0.033555$, Figure 8F). Additionally, a higher HPXscore was strikingly associated with excluded and immune-desert phenotypes in which ICIs had difficulty exerting an antitumor effect (Kruskal-Wallis test, $p = 0.00072$, Figure 8G). Additionally, patients with a lower HPXscore were more likely to benefit from ICI immunotherapy (Wilcoxon test, $p = 0.00011$, Figure S14I, and Kruskal-Wallis test, $p = 0.00028$, Figure 8I). In addition, the proportion of ICI treatment responders was significantly higher in patients with a low HPXscore compared with patients with a high HPXscore (Fisher's exact test, left, $p = 0.001091$; right, $p = 0.00011$, Figure 8H). Furthermore, we evaluated the predictive value of TMB, which is significantly associated with the efficacy of immunotherapy, with receiver operating characteristic (ROC) analysis in the IMvigor210 (mUC) cohort. However, we did not observe any difference in predictive advantage of TMB when compared with the HPXscore. Moreover, combination of TMB with the HPXscore could dramatically improve the predictive value compared with that of TMB or the HPXscore alone (Figure 8J). All of the above findings implied that the quantification of hypoxia response patterns was a robust biomarker for prognosis and potential predictor for clinical response in immunotherapy. In summary, our work strongly

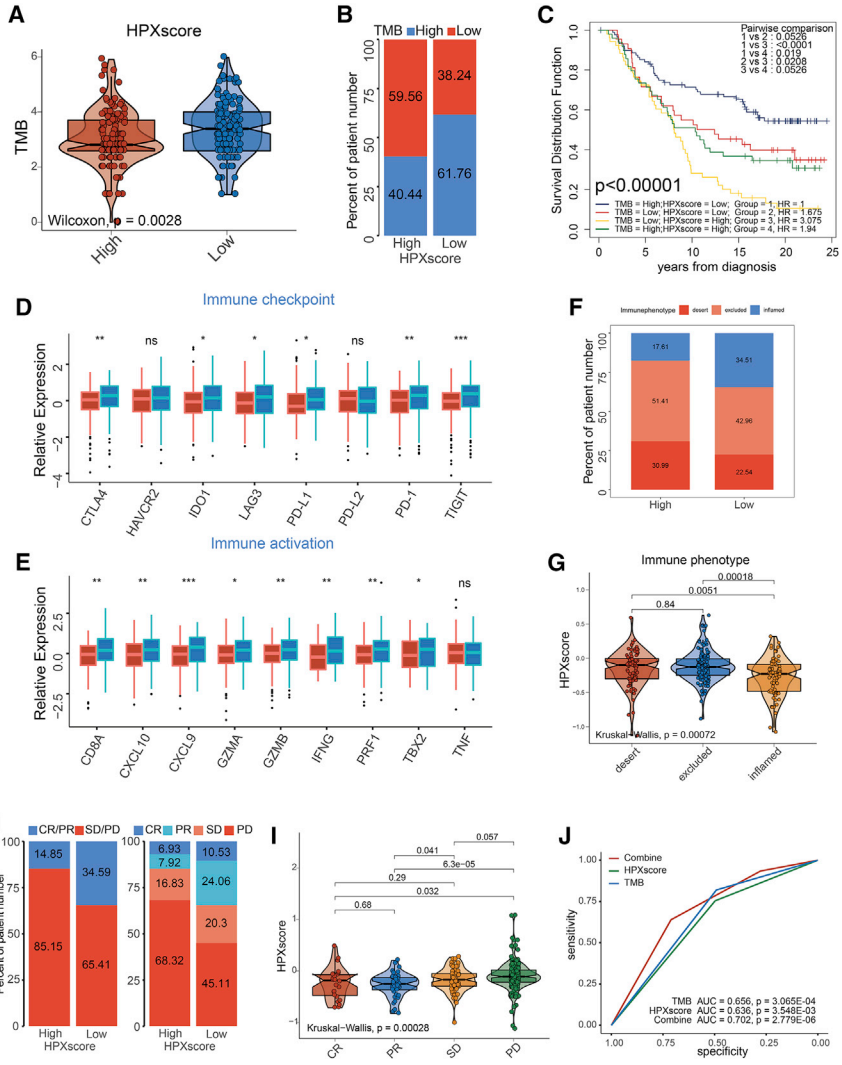

Figure 8. HPXscore was an efficiency tool for immunotherapy response prediction

(A) Difference in TMB between high and low HPXscore groups in the IMvigor210 (mUC) cohort. The TMB was log_2 transformed. The statistical difference was measured with the Wilcoxon test (p = 0.0028). (B) Proportion of TMB level in high and low HPXscore groups in the IMvigor210 (mUC) cohort. The statistical difference was measured with a Fisher's exact test (p = 0.001859). (C) Kaplan-Meier survival curves show the difference in prognosis advantage among four groups stratified by HPXscore and TMB in the IMvigor210 (mUC) cohort (log-rank test, p < 0.00001). (D and E) Difference in the expression of immune checkpoints (D) and immune activation-related genes (E) between high and low HPXscore groups in the IMvigor210 (mUC) cohort. The upper and lower ends of the boxes represent interquartile range of values. The lines in the boxes represent median value, and the black dots show outliers. The statistical difference between high and low HPXscore groups was tested by a Student's t test. *p < 0.05, **p < 0.01, ***p < 0.001. (F) The proportion of immune phenotypes between high and low HPXscore groups in the IMvigor210 (mUC) cohort. The statistical difference was measured with a Fisher's exact test (p = 0.033555). (G) Differences in HPXscore between different immune phenotypes in the IMvigor210 (mUC) cohort. The Kruskal-Wallis test was used to compare the statistical difference between different molecular subtypes (p = 0.00072). (H) Proportion of patients with response to ICI immunotherapy in low or high HPXscore groups in the IMvigor210 (mUC) cohort. CR, complete response; PR, partial response; SD, stable disease; PD, progressive disease. CR/PR was identified as responder, and SD/PD was identified as non-responder. The statistical difference was measured with a Fisher's exact test (left, p = 0.001091; right, p = 0.00317). (I) Differences in HPXscore between different ICI immunotherapy clinical response groups. The statistical difference was measured with the Kruskal-Wallis test (p = 0.00028). (J) Receiver-operating characteristic (ROC) curves measuring the predictive value of the HPXscore, TMB, and their combination in the IMvigor210 (mUC) cohort. The AUC was 0.636, 0.656, and 0.702 for the HPXscore, TMB, and HPXscore combined with TMB, respectively.

indicated that hypoxia response patterns were significantly associated with TME immune phenotypes and that the HPXscore would contribute to the prediction of response to ICI immunotherapy for individual.

DISCUSSION

Recently, cancer research has been transferred from only focusing on the tumor cells to the surroundings of core tumor cells, which is defined as the TME. The major components within the TME, including immune cells, stromal cells, as well as the chemokines and cytokines that they secrete, can collaborate with each other to exhibit a chronic inflammatory, immunosuppressive, and pro-tumoral environment to survive and protect tumors cells under strict immune surveillance.[33]

During cancer development and progression, tumor and TME cells might be permanently or transiently confronted with hypoxia according to a poor blood supply.[34] An aberrant vascularization-induced hypoxic region in tumors could trigger immune tolerance by creating a hostile hypoxic TME that can hamper antigen-presenting cell (APC) recognition and dampen the efficacy of effector immune cell-mediated elimination.[18,35] Moreover, tumor cells surrounded within a hypoxic TME are presumed to represent more aggressive and drug resistance phenotypes. Hypoxia-induced adaptive responses could concurrently activate various cellular pathways, resulting in cell plasticity, functional heterogeneity, immune suppression, and resistance to cytotoxicity.[36] In this regard, several essential elements of the hypoxia response pathway are good candidates for therapeutic targeting. As most studies only focused on a single hypoxia-related

gene, such as HIF1α and CA9, in regulating single or several TME cell types, the comprehensive analyses of hypoxia in mediating the TME immune cell infiltration are not fully identified. Determining the role of distinct hypoxia response patterns in the TME immune cell infiltration will help us to understand the underlying mechanism of the TME-related immune response and make current immunotherapy strategies more efficient.

In the present study, five distinct hypoxia response patterns have been identified through unsupervised consensus clustering. These five patterns exhibited different prognosis, TME immune cell infiltration, and biological pathway enrichment. In the meta-BLCA cohort, HPXclusterA was characterized by a high level of TME immune cell infiltration and activation of stroma-related pathways, and similar traits could also be seen in HPXclusterB. However, we found that HPXclusterA and HPXclusterB showed a high level of TME immune cell infiltration with a poor clinical outcome. It is well documented that appropriate localization and migration of T cells are essential elements for antitumor immune surveillance. The stromal status, which is referred to as "loose" or "dense," might significantly influence the migration of T cells and restrict them from entering tumor islets.[37] Due to the stromal-relevant pathway activation, immune cells cannot penetrate tumor parenchyma and were retained in the stroma surrounding core tumor nests in HPXclusterA and HPXclusterB, resulting in mismatched survival advantage, and they more likely corresponded to the immune-excluded phenotype. HPXclusterC and HPXclusterE were both featured with low TME immune cell infiltration, immunity suppression, and were referred to the immune-desert phenotype, which was associated with immune tolerance and ignorance, as well as lack of activated and priming T cells.[38] The immune-excluded and immune-desert phenotypes were regarded as non-inflamed tumors or immune-suppressed ("cold") tumors.[39] However, high effector TME immune cell infiltration and activation of adaptive immunity could be found in HPXclusterD, which were characteristics of immune-inflamed phenotype, also known as a "hot" tumor.[40] Consistent with the above definitions, our subsequent analyses showed that the angiogenesis, EMT, and pan-fibroblast TGF-β response pathways, which were responsible for stromal activation, were remarkably enriched, whereas the CD8 T effector, antigen-processing machinery, and immune checkpoint signatures, which were responsible for immune activation, were strikingly suppressed in HPXclusterA and HPXclusterB. However, the opposite patterns were observed in HPXclusterD. All of the above findings were also validated in the independent TCGA-BLCA cohort. With the combination of the characteristics of TME immune cell infiltration and biological pathway enrichment, the reliability of hypoxia response patterns in the identification and classification of immune phenotypes in BLCA was confirmed.

A growing body of evidence suggests that patients with a positive prognostic value more likely exhibit an immune-inflamed TME, especially in patients with advanced solid tumors, who will have a durable response and extended overall survival (OS) when receiving ICI immunotherapy.[38] However, not all patients treated with ICI-based therapy experience tumor shrinkage, a durable response, or prolonged survival. To extend such benefits to more cancer patients, it is necessary to understand the underlying mechanism of primary or secondary immune escape in these patients, which disenable the effector immune cells to eradicate the cancer cells. There are many factors related to immune escape such as poor TME immune cell infiltration into tumor parenchyma, dysregulation between effector immune cells (CD8 T cells) and immunosuppressive factors and cells (Treg cells) within the TME, downregulation of the MHC on cancer cells, and lack of strong cancer antigens or epitopes recognized by antigen-processing cells or T cells.[41] As our hypoxia response patterns were able to distinguish the distinct TME immune cell infiltration and immune phenotypes, we next determined whether our established patterns have some relationship with tumor mutation load. The recognition of neo-antigens induced by somatic nonsynonymous coding mutations was the main initiator for activation of adaptive immunity, and the mutation landscape is regarded as a potential biomarker for predicting the clinical responses to ICI immunotherapies.[42] Although the detection of overall neo-antigens is difficult, the TMB, which can be easily obtained and used to assess the neo-antigen load, has been proven to serve as good indicator for clinical benefits in predicting the ICI response.[43,44] In TCGA-BLCA cohort, we found that HPXclusterE, which is similar to HPXclusterD in the meta-BLCA cohort, displayed the highest mutated rate among five distinct hypoxia response patterns, especially for TP53 and RB1, which was regarded as a predictor for ICI treatment in some cases. Moreover, we also found that HPXclusterE was highly enriched in the mismatch repair signaling pathway, which might be attracted by high genetic mutation to conduct DNA/RNA repair, resulting in good prognosis. This may explain why HPXclusterE has a survival advantage compared with other clusters from another side. Current studies demonstrate that a high TMB might induce a durable clinical response to anti-PD-1/PD-L1 immunotherapy. Therefore, the above results indirectly demonstrate that HPXclusterE might be more sensitive to ICIs and that hypoxia response patterns could be an essential factor in regulating the clinical response to ICIs.

Furthermore, DEGs between distinct hypoxia response patterns were reported to be enriched in stromal and immune-related biological processes. Then, these DEGs were determined to be hypoxia phenotype-related genes. Considering individual heterogeneity, we established a set scoring system, referring to the hypoxia phenotype-related gene signature (HPXscore), to evaluate and quantify the hypoxia response pattern of individual with BLCA. We found that the low HPXscore group was enriched in immune activation-relevant pathways, which referred to an immune-inflamed phenotype, while the high HPXscore group was enriched in stromal-relevant pathways, which referred to an immune-excluded and immune-desert phenotype. In addition, these results were well validated in the IMvigor210 (mUC) cohort that immune-desert and excluded phenotypes showed a higher HPXscore, while the immune-inflamed phenotype exhibited a significantly lower HPXscore. Moreover, HPXclusterE, characterized by an immune-inflamed phenotype, showed the lowest HPXscore with better prognosis, where HPXclusterA showed the

highest HPXscore with poorer prognosis. All of these findings suggested that the HPXscore is a reliable and robust tool for comprehensive assessment of hypoxia response patterns in individualand could be used to further identify TME immune cell infiltration and tumor immune phenotypes. Moreover, patients with a high HPXscore were more inclined to be associated with high malignancy clinicopathological traits and molecular subtypes, while the opposite patterns were observed in the low HPXscore group. In addition, patients with GU and TCGA II subtypes, which were characterized by immune activation and more sensitivity to ICI immunotherapy, were strikingly associated with a low HPXscore. Meanwhile, patients with TCGA III/IV subtypes, which were featured by stromal activation and were less sensitive to ICI immunotherapy, were significantly correlated with a high HPXscore.[45,46] Previous studies demonstrated that TGF-β/EMT signaling activation could result in decreased priming of effector T cells into tumor parenchyma as well as hamper their cytotoxicity effects.[47] Additionally, we found that the ICI immunotherapy responders have a lower HPXscore, and patients with a lower HPXscore were more likely to benefit from ICI treatment. Consistent with a high mutation load existing in the GU subtype, the HPXscore was found to significantly negative correlated with TMB in both TCGA-BLCA and IMvigor210 (mUC) cohorts. We found that a combination of the HPXscore and TMB could dramatically improve predictive values when compared with the TMB or HPXscore alone. Furthermore, there was no difference in predictive advantage of TMB compared with HPXscore. This indicated that the response to ICI immunotherapy was a complicated process that was associated with many non-redundant factors, including (1) pre-existing immunity, characterized by antigen processing status and $CD8^+$ T effector activity; (2) TMB, directly measured by mutational variates, or indirectly reflected in signatures of mismatch repair response; and (3) TGF-β/EMT signaling in full activation. All of the above results suggested that our hypoxia response patterns and HPXscore, which might influence these three main factors, would contribute to the prediction of the clinical benefit to ICIs immunotherapy.

In conclusion, the HPXscore was reliable to comprehensively assess the hypoxia response patterns of individual with BLCA, and it was associated with clinical, cellular, and molecular features, including clinical stages, histological subtypes, TME immune cell infiltration, immune phenotypes, molecular subtypes, genetic variation, and tumor mutation landscape. Moreover, the HPXscore could act as an independent prognostic factor for BLCA patient prognosis, as well as a predictive factor for clinical response to ICI immunotherapy. More importantly, this study has yielded several novel insights for exploitation of hypoxia response signaling pathways for clinical application in BLCA.

MATERIALS AND METHODS

Data collection and processing

We systematically searched publicly available gene expression datasets for BLCA. Samples without complete prognosis information were removed from further evaluation. In total, 995 samples from four microarray datasets (GEO: GSE13507, GSE32548, GSE32894, and GSE48075) and one RNA-sequencing dataset (TCGA-BLCA) were merged as the meta-BLCA cohort in our study. All raw data and clinical information from microarray datasets were obtained from the Gene Expression Omnibus (GEO) database (https://www.ncbi.nlm.nih.gov/geo/). Then, the raw data in the microarray dataset were processed via robust multi-chip averaging (RMA) algorithm background correction, $\log_2$ transformation, quantile normalization, and annotation by the package Affy in R.[48] When several probes mapped to a single gene symbol, the highest expressed probe was annotated as the gene expression. The level 3 RNA-sequencing data for fragments per kilobase of transcript per million mapped reads (FPKM) for gene expression of TCGA-BLCA dataset were downloaded from the TCGA Genomic Data Commons (GDC) data portal (https://portal.gdc.cancer.gov/). The gene expression was annotated with the highest expression when multiple Ensembl IDs mapped to a single gene symbol in RNA-sequencing data. Then, FPKM values were transformed into transcripts per kilobase million (TPM), which are more similar to gene expression from microarrays and more comparable between samples.[49] The ComBat algorithm of package sva in R was utilized to reduce the likelihood of batch effects of non-biological technical biases from each dataset.[50] Clinical data and sample information for TCGA-BLCA dataset were obtained from UCSC Xena (https://xenabrowser.net/datapages/?hub=https://tcga.xenahubs.net:443) or supplemental information from Robertson et al.[51] Detailed information on clinicopathological characteristics in each dataset can be found in our previous study[52] or in Tables S12 and S13. TCGA-BLCA somatic mutation data were downloaded from the Genomic Data Commons (https://portal.gdc.cancer.gov/) using the package TCGAbiolinks in R.[53] The called somatic variants processed with the MuTect2 algorithm were utilized as the raw mutation count. The TMB per megabase of each sample was calculated as the total number of mutations counted in the whole exon territory with 38 Mb according to a previous study.[54] Moreover, the IMvigor210 (mUC) dataset from patients with mUC receiving PD-L1 inhibitor atezolizumab were also enrolled in our study to validate our findings. The raw transcriptomic and clinical data were retrieved from the IMvigor210 (mUC) dataset (http://research-pub.gene.com/IMvigor210CoreBiologies) using the package IMvigor in R.[45] The raw count was also transformed to TPM to represent gene expression in the IMvigor210 (mUC) dataset, which is more comparable to other datasets in our study. Detailed clinical information on the IMvigor210 (mUC) dataset can be found in Table S14. Data were analyzed with the R (version 3.5.2) and R Bioconductor packages.

Unsupervised consensus clustering for hypoxia response-related patterns

The gene set "Reactome cellular response to hypoxia" was downloaded from the Molecular Signatures Database (MSigDB) of the Broad Institute (https://www.gsea-msigdb.org/gsea/msigdb/index.jsp). The unsupervised consensus clustering method (K-means) for analysis of hypoxia response-related genes was applied to identify distinct hypoxia response patterns (HPXcluster) based on Euclidean distance and Ward's linkage.[55] A consensus clustering algorithm was utilized to determine the number of clusters in the meta-BLCA cohort

and further validated in TCGA-BLCA cohort. This procedure was performed and repeated 1,000 times to guarantee the stability of classification using the package ConsensusClusterPlus in R.[56]

Identification of DEGs between hypoxia response patterns

According to the consensus clustering, we could successfully classify patients into five distinct hypoxia response patterns based on the expression of hypoxia response-related genes. DEGs between each pattern were determined by comparing the indicated pattern with all other patterns by using the package limma in R,[57] which estimates gene expression changes by implementing an empirical Bayesian approach. The significance criteria for determining DEGs were set as a false discovery rate (FDR) < 0.05 and $|\log_2$ fold change (FC)$|$ > 1.0.

Evaluation of infiltrating immune cells in the TME

ssGSEA is a non-parametric and unsupervised algorithm to analyze the variation in pathway and biological process activity in a single sample of a gene expression dataset. ssGSEA is focused on gene sets, which are groups of genes that share common biological function, chromosomal location, or regulation.[58] In this study, we used the ssGSEA algorithm to evaluate the relative amount of infiltrating immune cells in the BLCA TME. The marker gene sets for TME infiltration immune cell types were obtained and merged from the studies of Bindea et al.[59] and Charoentong et al.[60] (Table S15). Both innate immune cells (e.g., DCs, eosinophils, mast cells, macrophages, natural killer cells, neutrophils) and adaptive immune cells (e.g., B cells, T cells, T helper cells, $CD8^+$ T cells, Treg cells, and cytotoxic cells) were investigated. The normalized enrichment score (NES) calculated by ssGSEA was used to represent the relative amount of each TME infiltrating cell in BLCA. Endothelial cell and fibroblast infiltration was calculated by using the package MCPcounter in R.[61]

Functional and pathway enrichment analyses

Gene-annotation enrichment analyses were used to investigate the differences in biological processes between distinct hypoxia response patterns through the package clusterProfiler in R.[62] The significant differential GO terms were defined with a strict cut-off of $p < 0.01$, and the top 10 terms were selected to visualize. We performed a ssGSEA algorithm to identify the difference in biological process between distinct hypoxia response phenotypes using the GSVA (gene set variation analysis) package in R.[63] The gene sets of c2.cp.kegg.v6.2.symbols were downloaded from the MSigDB of the Broad Institute (https://www.gsea-msigdb.org/gsea/msigdb/index.jsp). In spite of measuring the KEGG signaling pathway, we also curated a set of gene sets to represent specific biological processes, which was constructed by Mariathasan et al.,[45] including (1) angiogenesis; (2) antigen processing machinery; (3) base excision repair; (4) CD8 T effectors; (5) cell cycle; (6) cell cycle regulators; (7) DNA damage repair 1 and 2; (8) DNA replication; (9) EMT, including EMT1, EMT2, and EMT3; (10) Fanconi anemia; (11) homologous recombination; (12) immune checkpoint; (13) mismatch repair; (14) nucleotide excision repair; (15) pan-fibroblast TGF-β response signature (pan-F-TBRS); and (16) WNT targets (Table S16).[45,46,64] A correlation analysis was further performed to reveal the association between distinct hypoxia response phenotypes and the above-related biological pathways signature.

Establishment of hypoxia phenotype-related gene signature

We established a scoring system, termed as hypoxia phenotype-related gene signature (HPXscore), to evaluate the hypoxia response pattern of individuals with BLCA. The procedures for establishment of the HPXscore were as follows: DEGs were identified from different HPXclusters and merged as the meta-DEGs. The meta-DEGs with significant prognosis differences were extracted as the candidate DEGs for further analysis by using univariate Cox regression analysis. Then, LASSO-Cox regression analysis based on the package *glmnet* in R was applied to build an optimal hypoxia phenotype-related gene signature for BLCA.[65] The Cox regression model with LASSO was used for dimension reduction to reduce noise or redundant genes. The optimal values of the penalty parameter λ were determined through 10 cross-validations. The HPXscore of our model for each sample was defined by the relative expression of each hypoxia phenotype-related gene and its associated Cox coefficient. The HPXscore = $\sum_{i=1}^{n}(\mathrm{coef}_i \times \mathrm{Expr}_i)$, where Expr_i is the relative expression of the gene in the signature for patient i and coef_i is the LASSO-Cox coefficient of gene i.

Statistical analyses

The statistical significance of variables between two groups was estimated by Student's t tests or Wilcoxon tests. In addition, for variables in more than two groups, one-way ANOVA or Kruskal-Wallis tests were used. The χ^2 test was applied to analyze correlations between the HPXscore and clinicopathological parameters. Kaplan-Meier survival curves were generated to calculate survival rates, and the significant differences between survival curves were determined with the log-rank test using the package survminer in R. Correlation coefficients between TME-infiltrating immune cells, distinct gene sets, and the HPXscore were computed by Pearson and distance correlation analyses. A two-sided Fisher's exact test was used to analyze contingency tables. Univariate and multivariate Cox proportional hazard models were used to estimate the hazard ratios (HRs) of variables and determine independent prognostic factors and were visualized with the package forestplot in R. A nomogram and calibration curves were generated with the packages rms, nomogramEx, and regplot in R. DCA was performed to determine whether our established nomogram was suitable for clinical use according to the suggestion of Iasonos et al.[66] A waterfall plot was used to present the mutation landscape in patients with distinct hypoxia response phenotypes in TCGA-BLCA cohort via packages maftools[67] and complexheatmap[68] in R. The package pROC in R was used to plot and visualize ROC curves. The area under the curve (AUC) and confidence intervals were utilized to evaluate the diagnostic accuracy of TMB, HPXscore, and their combination. All statistical analyses were performed with R software 3.5.3. Statistical significance was set at $p < 0.05$.

SUPPLEMENTAL INFORMATION

Supplemental information can be found online at https://doi.org/10.1016/j.omto.2021.06.011.

ACKNOWLEDGMENTS

The authors are grateful for the invaluable support and useful discussions with members in Department of Urology. We thank TCGA and GEO databases as well as the IMvigor210 package for the availability of the data. This work was supported by grants from National Natural Science Foundation of China (no. 81802550), the Beijing Natural Science Foundation (no. 7194279), the China Postdoctoral Science Foundation (no. 2019M660041), and the Beijing Postdoctoral Research Foundation (no. ZZ2019-04).

AUTHOR CONTRIBUTIONS

R.C. and L.Y. made substantial contributions to the conception and design of the research. R.C., L.Y., and B.M. integrated and analyzed the data. R.C., L.Y., and Y.T. wrote the paper. R.C., L.Y., B.M., G.W., Y.X., and T.Y. edited the manuscript and provided critical comments. All authors read and approved the final manuscript.

DECLARATION OF INTERESTS

The authors declare no competing interests.

REFERENCES

1. Bray, F., Ferlay, J., Soerjomataram, I., Siegel, R.L., Torre, L.A., and Jemal, A. (2018). Global cancer statistics 2018: GLOBOCAN estimates of incidence and mortality worldwide for 36 cancers in 185 countries. CA Cancer J. Clin. *68*, 394–424.
2. Morales, A., Eidinger, D., and Bruce, A.W. (1976). Intracavitary bacillus Calmette-Guerin in the treatment of superficial bladder tumors. J. Urol. *116*, 180–183.
3. Meeks, J.J., Al-Ahmadie, H., Faltas, B.M., Taylor, J.A., 3rd, Flaig, T.W., DeGraff, D.J., Christensen, E., Woolbright, B.L., McConkey, D.J., and Dyrskjøt, L. (2020). Genomic heterogeneity in bladder cancer: Challenges and possible solutions to improve outcomes. Nat. Rev. Urol. *17*, 259–270.
4. Bhat, A., and Ritch, C.R. (2019). Urinary biomarkers in bladder cancer: Where do we stand? Curr. Opin. Urol. *29*, 203–209.
5. Aine, M., Eriksson, P., Liedberg, F., Höglund, M., and Sjödahl, G. (2015). On molecular classification of bladder cancer: Out of one, many. Eur. Urol. *68*, 921–923.
6. Sjödahl, G., Lauss, M., Lövgren, K., Chebil, G., Gudjonsson, S., Veerla, S., Patschan, O., Aine, M., Fernö, M., Ringnér, M., et al. (2012). A molecular taxonomy for urothelial carcinoma. Clin. Cancer Res. *18*, 3377–3386.
7. Damrauer, J.S., Hoadley, K.A., Chism, D.D., Fan, C., Tiganelli, C.J., Wobker, S.E., Yeh, J.J., Milowsky, M.I., Iyer, G., Parker, J.S., and Kim, W.Y. (2014). Intrinsic subtypes of high-grade bladder cancer reflect the hallmarks of breast cancer biology. Proc. Natl. Acad. Sci. USA *111*, 3110–3115.
8. Choi, W., Porten, S., Kim, S., Willis, D., Plimack, E.R., Hoffman-Censits, J., Roth, B., Cheng, T., Tran, M., Lee, I.L., et al. (2014). Identification of distinct basal and luminal subtypes of muscle-invasive bladder cancer with different sensitivities to frontline chemotherapy. Cancer Cell *25*, 152–165.
9. Cancer Genome Atlas Research Network (2014). Comprehensive molecular characterization of urothelial bladder carcinoma. Nature *507*, 315–322.
10. Hanahan, D., and Coussens, L.M. (2012). Accessories to the crime: Functions of cells recruited to the tumor microenvironment. Cancer Cell *21*, 309–322.
11. Gajewski, T.F., Schreiber, H., and Fu, Y.X. (2013). Innate and adaptive immune cells in the tumor microenvironment. Nat. Immunol. *14*, 1014–1022.
12. Semenza, G.L. (2012). Hypoxia-inducible factors in physiology and medicine. Cell *148*, 399–408.
13. Keith, B., and Simon, M.C. (2007). Hypoxia-inducible factors, stem cells, and cancer. Cell *129*, 465–472.
14. Majmundar, A.J., Wong, W.J., and Simon, M.C. (2010). Hypoxia-inducible factors and the response to hypoxic stress. Mol. Cell *40*, 294–309.
15. Gilkes, D.M., Semenza, G.L., and Wirtz, D. (2014). Hypoxia and the extracellular matrix: Drivers of tumour metastasis. Nat. Rev. Cancer *14*, 430–439.
16. Semenza, G.L. (2010). Defining the role of hypoxia-inducible factor 1 in cancer biology and therapeutics. Oncogene *29*, 625–634.
17. Jayaprakash, P., Ai, M., Liu, A., Budhani, P., Bartkowiak, T., Sheng, J., Ager, C., Nicholas, C., Jaiswal, A.R., Sun, Y., et al. (2018). Targeted hypoxia reduction restores T cell infiltration and sensitizes prostate cancer to immunotherapy. J. Clin. Invest. *128*, 5137–5149.
18. Jing, X., Yang, F., Shao, C., Wei, K., Xie, M., Shen, H., and Shu, Y. (2019). Role of hypoxia in cancer therapy by regulating the tumor microenvironment. Mol. Cancer *18*, 157.
19. Vokes, E.E., Ready, N., Felip, E., Horn, L., Burgio, M.A., Antonia, S.J., Arén Frontera, O., Gettinger, S., Holgado, E., Spigel, D., et al. (2018). Nivolumab versus docetaxel in previously treated advanced non-small-cell lung cancer (CheckMate 017 and CheckMate 057): 3-Year update and outcomes in patients with liver metastases. Ann. Oncol. *29*, 959–965.
20. Sharma, P., Retz, M., Siefker-Radtke, A., Baron, A., Necchi, A., Bedke, J., Plimack, E.R., Vaena, D., Grimm, M.O., Bracarda, S., et al. (2017). Nivolumab in metastatic urothelial carcinoma after platinum therapy (CheckMate 275): A multicentre, single-arm, phase 2 trial. Lancet Oncol. *18*, 312–322.
21. Larkin, J., Minor, D., D'Angelo, S., Neyns, B., Smylie, M., Miller, W.H., Jr., Gutzmer, R., Linette, G., Chmielowski, B., Lao, C.D., et al. (2018). Overall survival in patients with advanced melanoma who received nivolumab versus investigator's choice chemotherapy in CheckMate 037: A randomized, controlled, open-label phase III trial. J. Clin. Oncol. *36*, 383–390.
22. Ho, P.C., Bihuniak, J.D., Macintyre, A.N., Staron, M., Liu, X., Amezquita, R., Tsui, Y.C., Cui, G., Micevic, G., Perales, J.C., et al. (2015). Phosphoenolpyruvate is a metabolic checkpoint of anti-tumor t cell responses. Cell *162*, 1217–1228.
23. Barsoum, I.B., Smallwood, C.A., Siemens, D.R., and Graham, C.H. (2014). A mechanism of hypoxia-mediated escape from adaptive immunity in cancer cells. Cancer Res. *74*, 665–674.
24. Chouaib, S., Noman, M.Z., Kosmatopoulos, K., and Curran, M.A. (2017). Hypoxic stress: Obstacles and opportunities for innovative immunotherapy of cancer. Oncogene *36*, 439–445.
25. Facciabene, A., Peng, X., Hagemann, I.S., Balint, K., Barchetti, A., Wang, L.P., Gimotty, P.A., Gilks, C.B., Lal, P., Zhang, L., and Coukos, G. (2011). Tumour hypoxia promotes tolerance and angiogenesis via CCL28 and T_{reg} cells. Nature *475*, 226–230.
26. Noman, M.Z., Desantis, G., Janji, B., Hasmim, M., Karray, S., Dessen, P., Bronte, V., and Chouaib, S. (2014). PD-L1 is a novel direct target of HIF-1α, and its blockade under hypoxia enhanced MDSC-mediated T cell activation. J. Exp. Med. *211*, 781–790.
27. Corzo, C.A., Condamine, T., Lu, L., Cotter, M.J., Youn, J.I., Cheng, P., Cho, H.I., Celis, E., Quiceno, D.G., Padhya, T., et al. (2010). HIF-1α regulates function and differentiation of myeloid-derived suppressor cells in the tumor microenvironment. J. Exp. Med. *207*, 2439–2453.
28. Chen, D.S., and Mellman, I. (2017). Elements of cancer immunity and the cancer-immune set point. Nature *541*, 321–330.
29. Qian, C., and Cao, X. (2018). Dendritic cells in the regulation of immunity and inflammation. Semin. Immunol. *35*, 3–11.
30. Kim, S.S., Harford, J.B., Moghe, M., Slaughter, T., Doherty, C., and Chang, E.H. (2019). A tumor-targeting nanomedicine carrying the p53 gene crosses the blood-brain barrier and enhances anti-PD-1 immunotherapy in mouse models of glioblastoma. Int. J. Cancer *145*, 2535–2546.
31. Knudsen, E.S., Pruitt, S.C., Hershberger, P.A., Witkiewicz, A.K., and Goodrich, D.W. (2019). Cell cycle and beyond: Exploiting new RB1 controlled mechanisms for cancer therapy. Trends Cancer *5*, 308–324.
32. Glaser, A.P., Fantini, D., Wang, Y., Yu, Y., Rimar, K.J., Podojil, J.R., Miller, S.D., and Meeks, J.J. (2017). APOBEC-mediated mutagenesis in urothelial carcinoma is

associated with improved survival, mutations in DNA damage response genes, and immune response. Oncotarget *9*, 4537–4548.

33. Wu, T., and Dai, Y. (2017). Tumor microenvironment and therapeutic response. Cancer Lett. *387*, 61–68.
34. Sormendi, S., and Wielockx, B. (2018). Hypoxia pathway proteins as central mediators of metabolism in the tumor cells and their microenvironment. Front. Immunol. *9*, 40.
35. Casey, S.C., Amedei, A., Aquilano, K., Azmi, A.S., Benencia, F., Bhakta, D., Bilsland, A.E., Boosani, C.S., Chen, S., Ciriolo, M.R., et al. (2015). Cancer prevention and therapy through the modulation of the tumor microenvironment. Semin. Cancer Biol. *35* (*Suppl*), S199–S223.
36. Qian, J., and Rankin, E.B. (2019). Hypoxia-induced phenotypes that mediate tumor heterogeneity. Adv. Exp. Med. Biol. *1136*, 43–55.
37. Salmon, H., Franciszkiewicz, K., Damotte, D., Dieu-Nosjean, M.C., Validire, P., Trautmann, A., Mami-Chouaib, F., and Donnadieu, E. (2012). Matrix architecture defines the preferential localization and migration of T cells into the stroma of human lung tumors. J. Clin. Invest. *122*, 899–910.
38. Kim, J.M., and Chen, D.S. (2016). Immune escape to PD-L1/PD-1 blockade: Seven steps to success (or failure). Ann. Oncol. *27*, 1492–1504.
39. Lowe, K.L., Cole, D., Kenefeck, R., OKelly, I., Lepore, M., and Jakobsen, B.K. (2019). Novel TCR-based biologics: Mobilising T cells to warm "cold" tumours. Cancer Treat. Rev. *77*, 35–43.
40. Gajewski, T.F. (2015). The next hurdle in cancer immunotherapy: Overcoming the non-T-cell-inflamed tumor microenvironment. Semin. Oncol. *42*, 663–671.
41. Gajewski, T.F., Woo, S.R., Zha, Y., Spaapen, R., Zheng, Y., Corrales, L., and Spranger, S. (2013). Cancer immunotherapy strategies based on overcoming barriers within the tumor microenvironment. Curr. Opin. Immunol. *25*, 268–276.
42. Fancello, L., Gandini, S., Pelicci, P.G., and Mazzarella, L. (2019). Tumor mutational burden quantification from targeted gene panels: Major advancements and challenges. J. Immunother. Cancer *7*, 183.
43. Rizvi, N.A., Hellmann, M.D., Snyder, A., Kvistborg, P., Makarov, V., Havel, J.J., Lee, W., Yuan, J., Wong, P., Ho, T.S., et al. (2015). Mutational landscape determines sensitivity to PD-1 blockade in non-small cell lung cancer. Science *348*, 124–128.
44. Gibney, G.T., Weiner, L.M., and Atkins, M.B. (2016). Predictive biomarkers for checkpoint inhibitor-based immunotherapy. Lancet Oncol. *17*, e542–e551.
45. Mariathasan, S., Turley, S.J., Nickles, D., Castiglioni, A., Yuen, K., Wang, Y., Kadel, E.E., III, Koeppen, H., Astarita, J.L., Cubas, R., et al. (2018). TGFβ attenuates tumour response to PD-L1 blockade by contributing to exclusion of T cells. Nature *554*, 544–548.
46. Rosenberg, J.E., Hoffman-Censits, J., Powles, T., van der Heijden, M.S., Balar, A.V., Necchi, A., Dawson, N., O'Donnell, P.H., Balmanoukian, A., Loriot, Y., et al. (2016). Atezolizumab in patients with locally advanced and metastatic urothelial carcinoma who have progressed following treatment with platinum-based chemotherapy: A single-arm, multicentre, phase 2 trial. Lancet *387*, 1909–1920.
47. Tauriello, D.V.F., Palomo-Ponce, S., Stork, D., Berenguer-Llergo, A., Badia-Ramentol, J., Iglesias, M., Sevillano, M., Ibiza, S., Cañellas, A., Hernando-Momblona, X., et al. (2018). TGFβ drives immune evasion in genetically reconstituted colon cancer metastasis. Nature *554*, 538–543.
48. Gautier, L., Cope, L., Bolstad, B.M., and Irizarry, R.A. (2004). affy—Analysis of Affymetrix GeneChip data at the probe level. Bioinformatics *20*, 307–315.
49. Wagner, G.P., Kin, K., and Lynch, V.J. (2012). Measurement of mRNA abundance using RNA-seq data: RPKM measure is inconsistent among samples. Theory Biosci *131*, 281–285.
50. Johnson, W.E., Li, C., and Rabinovic, A. (2007). Adjusting batch effects in microarray expression data using empirical Bayes methods. Biostatistics *8*, 118–127.
51. Robertson, A.G., Kim, J., Al-Ahmadie, H., Bellmunt, J., Guo, G., Cherniack, A.D., Hinoue, T., Laird, P.W., Hoadley, K.A., Akbani, R., et al.; TCGA Research Network (2017). Comprehensive molecular characterization of muscle-invasive bladder cancer. Cell *171*, 540–556.e25.
52. Cao, R., Yuan, L., Ma, B., Wang, G., Qiu, W., and Tian, Y. (2020). An EMT-related gene signature for the prognosis of human bladder cancer. J. Cell. Mol. Med. *24*, 605–617.
53. Colaprico, A., Silva, T.C., Olsen, C., Garofano, L., Cava, C., Garolini, D., Sabedot, T.S., Malta, T.M., Pagnotta, S.M., Castiglioni, I., et al. (2016). TCGAbiolinks: An R/Bioconductor package for integrative analysis of TCGA data. Nucleic Acids Res. *44*, e71.
54. Chalmers, Z.R., Connelly, C.F., Fabrizio, D., Gay, L., Ali, S.M., Ennis, R., Schrock, A., Campbell, B., Shlien, A., Chmielecki, J., et al. (2017). Analysis of 100,000 human cancer genomes reveals the landscape of tumor mutational burden. Genome Med. *9*, 34.
55. Nidheesh, N., Abdul Nazeer, K.A., and Ameer, P.M. (2017). An enhanced deterministic K-means clustering algorithm for cancer subtype prediction from gene expression data. Comput. Biol. Med. *91*, 213–221.
56. Monti, S., Tamayo, P., Mesirov, J., and Golub, T. (2003). Consensus clustering: A resampling-based method for class discovery and visualization of gene expression microarray data. Mach. Learn. *52*, 91–118.
57. Ritchie, M.E., Phipson, B., Wu, D., Hu, Y., Law, C.W., Shi, W., and Smyth, G.K. (2015). limma powers differential expression analyses for RNA-sequencing and microarray studies. Nucleic Acids Res. *43*, e47.
58. Subramanian, A., Tamayo, P., Mootha, V.K., Mukherjee, S., Ebert, B.L., Gillette, M.A., Paulovich, A., Pomeroy, S.L., Golub, T.R., Lander, E.S., and Mesirov, J.P. (2005). Gene set enrichment analysis: A knowledge-based approach for interpreting genome-wide expression profiles. Proc. Natl. Acad. Sci. USA *102*, 15545–15550.
59. Bindea, G., Mlecnik, B., Tosolini, M., Kirilovsky, A., Waldner, M., Obenauf, A.C., Angell, H., Fredriksen, T., Lafontaine, L., Berger, A., et al. (2013). Spatiotemporal dynamics of intratumoral immune cells reveal the immune landscape in human cancer. Immunity *39*, 782–795.
60. Charoentong, P., Finotello, F., Angelova, M., Mayer, C., Efremova, M., Rieder, D., Hackl, H., and Trajanoski, Z. (2017). Pan-cancer immunogenomic analyses reveal genotype-immunophenotype relationships and predictors of response to checkpoint blockade. Cell Rep. *18*, 248–262.
61. Becht, E., Giraldo, N.A., Lacroix, L., Buttard, B., Elarouci, N., Petitprez, F., Selves, J., Laurent-Puig, P., Sautès-Fridman, C., Fridman, W.H., and de Reyniès, A. (2016). Estimating the population abundance of tissue-infiltrating immune and stromal cell populations using gene expression. Genome Biol. *17*, 218.
62. Yu, G., Wang, L.G., Han, Y., and He, Q.Y. (2012). clusterProfiler: An R package for comparing biological themes among gene clusters. OMICS *16*, 284–287.
63. Hänzelmann, S., Castelo, R., and Guinney, J. (2013). GSVA: Gene set variation analysis for microarray and RNA-seq data. BMC Bioinformatics *14*, 7.
64. Şenbabaoğlu, Y., Gejman, R.S., Winer, A.G., Liu, M., Van Allen, E.M., de Velasco, G., Miao, D., Ostrovnaya, I., Drill, E., Luna, A., et al. (2016). Tumor immune microenvironment characterization in clear cell renal cell carcinoma identifies prognostic and immunotherapeutically relevant messenger RNA signatures. Genome Biol. *17*, 231.
65. Friedman, J., Hastie, T., and Tibshirani, R. (2010). Regularization paths for generalized linear models via coordinate descent. J. Stat. Softw. *33*, 1–22.
66. Iasonos, A., Schrag, D., Raj, G.V., and Panageas, K.S. (2008). How to build and interpret a nomogram for cancer prognosis. J. Clin. Oncol. *26*, 1364–1370.
67. Mayakonda, A., Lin, D.C., Assenov, Y., Plass, C., and Koeffler, H.P. (2018). Maftools: Efficient and comprehensive analysis of somatic variants in cancer. Genome Res. *28*, 1747–1756.
68. Gu, Z., Eils, R., and Schlesner, M. (2016). Complex heatmaps reveal patterns and correlations in multidimensional genomic data. Bioinformatics *32*, 2847–2849.